Chapter 8

Multidector CT Imaging of Coronary Artery Stent and Coronary Artery Bypass Graft

Bong Gun Song

Additional information is available at the end of the chapter

http://dx.doi.org/10.5772/54085

1. Introduction

Coronary artery stenting has become the most important nonsurgical treatment for coronary artery disease. However, in-stent restenosis occurs at a relatively high rate and this problem has led to the routine use of invasive angiography for assessing stent patency. Although coronary angiography is the clinical gold standard and it is a very effective diagnostic tool for detecting such in-stent restenosis, it's clearly an invasive procedure with its associated morbidity and mortality risks. Therefore, a noninvasive technique for detecting in-stent restenosis would be of great interest and use for following up patients after coronary angioplasty. Multidetector-row CT (MDCT) is being increasingly used for noninvasive coronary artery imaging as it has high diagnostic accuracy for detecting coronary artery stenosis in native, non-stented, coronary arteries. The recently introduced 64-slice CT offers more improved spatial and temporal resolution than does 4 and 16-slice CT and this results in superior visualization of the stent lumen and in-stent restenosis. However, although 64-slice MDCT allows for improved stent visualization, a relevant part (up to 47%) of the stent lumen is still not assessable (Mahnken et al., 2006). The metal of the stents can cause blooming artifacts that prevent the accurate interpretation of a lumen's patency. To improve a stent's visualization, numerous methods have been attempted such as dedicated post-processing or the use of dual-source CT. However, because of its presently limited sensitivity and high radiation exposure, MDCT should not be used as the first-line test to screen for in-stent restenosis in asymptomatic patients. Given its high specificity and negative predictive value, MDCT might be valuable for confirming stent occlusion in symptomatic patients.

Coronary artery bypass graft (CABG) surgery is the standard care in the treatment of advanced coronary artery disease. Notwithstanding the clear benefits of bypass grafting, recurrent chest pain after myocardial revascularization surgery is a common postoperative

presentation and the long-term clinical outcome after myocardial revascularization surgery is largely dependent on graft patency and the progression of coronary artery disease. Therefore, assessment of the status of the grafts and graft disease after CABG surgery is an important issue in cardiology. Although conventional coronary angiography is still standard method for assessment of the status of naïve and recipient vessels after CABG surgery, it is an invasive and costly procedure that is not risk-free. Recently, MDCT with retrospective electrocardiographic (ECG) gating has gained rapid acceptance as a diagnostic cardiac imaging modality, allowing assessment of coronary bypass graft patency with high spatial resolution. Initial assessment of bypass grafts was done with single-slice scanners and electron-beam CT. Subsequently, the addition of electrocardiographic (ECG) gating and the improved capabilities available with 4- or 16-slice MDCT scanners for rapid scanning of the area of interest led to promising results in the imaging of bypass grafts (Marano et al., 2005; Ueyama et al., 1999). Recently, the introduction of 64-slice MDCT permitted improved temporal resolution (94 to 200 msec) and spatial resolution (upto submillimeter) and reduction of both cardiac and respiratory motion, leading to improved assessment of graft stenosis and occlusion (Frazier et al., 2005; Lee et al., 2010). Moreover, 3-dimensional (3D) image processing and advanced volumetric visualization techniques now allow radiologists and cardiologists to evaluate coronary grafts in multiple planes using various projections. With the capability of acquiring 3D data volumes along with its tomographic nature, it shares many of the advantages of intravascular ultrasound and thus has the potential to enhance the practice of percutaneous coronary intervention (PCI) in the catheterization laboratory by providing data which was difficult to obtain by invasive coronary angiography (Song et al., 2010; Dikkers et al., 2007; Vembar et al., 2003). MDCT scanners characterized by submillimeter spatial resolution and a temporal resolution of 94 to 200 ms are now available and are increasingly used for cardiac imaging with promising results.

2. Imaging acquisition

2.1. Image protocol

Cardiac CTA technique requires rapid injection of nonionic, iodinated, low-osmolar intravenous contrast. A bolus of 100 to 120 mL nonionic contrast material (high iodine concentration is recommended) is administered intravenously using an automatic injector at a flow rate of 3 to 4 mL/s. A region of interest was placed in the descending aorta by using a preset threshold of 150 HU; a 10-second delay followed before scanning was begun to ensure filling of the distal vessels with contrast material. Axial images are reconstructed in the mid-to-late diastolic phase, using a fraction (percentage; relative delay) of the R-R interval of the cardiac cycle. Images are acquired with a heart rate < 70 beats per minute, if possible, and with breath-holding during mid-inspiration to prevent substantial inflow of unopacified blood into the right atrium, which may result in heterogeneity of contrast. Low heart rates (< 65 beats/min for 16-slice MDCT or < 70 beats/min for 64-slice MDCT) are recommended to obtain high-quality CT scans, and in the absence of contraindications (heart failure, systolic BP < 100 mm Hg, atrioventricular blockade greater than grade I, and referred adverse reac-

http://dx.doi.org/10.5772/54085

tion), beta-blockers can be administered before CT acquisition (Frazier et al., 2005; Marano et al., 2005). Oral or intravenous beta-adrenergic blocking medications, specifically metoprolol (Lopressor; Novartis Pharmaceuticals Corp., East Hanover, NJ), are administered prior to scanning to prevent heart rate variabilityand tachycardia. Retrospective ECG-gated CTA is essential for optimal image acquisition and reconstruction of evenly spaced phases of the cardiac cycle. The images are acquired in a limited field of view with axial images centered on the heart. Using 60% to 80% of the R-R interval, with 0.6-0.75 mm thick images reconstructed in 0.4-0.5 mm increments, axial source images, three-dimensional (3D) volume-rendered images, and multiplanar reformatted (MPR) images are generated.

There are a variety of protocols for image acquisition in the evaluation of patients after CABG surgery. In many respects, the protocol is similar to that for coronary CT angiography (CTA). One important difference is that the scan should be extended superiorly to include the origins of the internal mammary arteries. Scanning is performed with the patient in the supine position, during breath-hold. After placement of the leads for ECG recording on the chest wall and a check of the heart rate, a noncontrast CT scan image is acquired through the entire thorax in order to define the volume of the subsequent CT angiography and to detect associated or unsuspected findings. Hence, MDCT angiography is performed during ECG recording, from the subclavian arteries to the cardiac base; in patients with venous grafts, a smaller scanning volume starting from the lower third of the ascending aorta is usually sufficient. On the contrary, when a right gastroepiploic artery (RGEA) has been used, the scanning volume should include the upper abdomen. Since the left internal mammary artery (LIMA) is the most frequently used graft to the anterior cardiac wall, a right arm venous access is preferable in order to avoid streak artifacts from the left subclavian vein that may hamper a complete evaluation of LIMA course and takeoff. Both 3D volume-rendering and MPR images are used to assess the bypass grafts, proximal and/or distal graft anastomoses, and the cardiac anatomy. In particular, curved multiplanar images with centerlines through the bypass grafts and native coronary arteries are obtained. To correctly assess graft patency and/or the presence of significant stenosis and occlusion, a thorough knowledge of CABG anatomy and its configuration on CTA is important for radiologists and cardiologists. There are 2 types of bypass grafts, arterial and venous. Venous grafts are generally larger in caliber than arterial grafts, and for this reason, jointly to the absence of surgical clips along their course, venous grafts are usually better assessable by noninvasive imaging techniques. In order of frequency of use, graft arteries include the internal mammary arteries (IMAs), radial arteries (RAs), right gastroepiploic artery (RGEA), and inferior epigastric artery. Although arterial grafts have better long-term outcomes, venous grafts, specifically saphenous vein grafts (SVGs), are more readily available. CTA following CABG surgery is done by first assessing the morphology and size of the ascending aorta and the origin of the in situ vessel such as the IMA. Then, graft patency is assessed for homogeneous, contrast-enhanced graft lumen and for regular shape and border of the graft wall. The graft is usually divided into 3 different segments: the origin or proximal anastomosis of the graft, the body of the graft, and the single (or sequential) distal anastomosis. During the CTA evaluation of bypass grafts, the proximal anastomosis is usually better visualized than

the distal anastomosis. In cases in which the distal anastomosis is not well evaluated, the bypass graft is usually considered patent as long as contrast is evident within the graft lumen.

2.2. Image noise

The advantages of MDCT are the relatively rapid imaging time and high spatial resolution attributable to the multi-row detector system. Numerous studies dealing with MDCT coronary bypass angiography have reported cardiac and respiratory motion artifacts as the most significant limitations in the reliable assessment of graft patency and stenosis of recipient vessels. It is well known that heart rate greatly influences image quality and stenosis detection. The introduction of 64-slice MDCT scanners, with faster gantry rotation times and shorter breath-hold times, improved diagnostic image quality by reducing cardiac and respiratory motion artifacts. However, optimum performance was observed primarily in patients with heart rates below 70 beats per minute. Even with improved spatial and temporal resolution with 64-slice technology, routine administration of β-blockers is still required. If graft segment image quality is suboptimal due to motion artifacts, a potential remedy is to obtain additional image reconstructions in smaller increments throughout the cardiac cycle. The other limitations of MDCT are the presence of calcification and metal clip artifacts, which make assessment of graft patency difficult, and accurate evaluation of the degree of stenosis impossible. Nevertheless, the thinner slices of 64-slice MDCT give increased temporal resolution, and 3-dimentional reconstructions show consistent detail in every plane. Moreover, bypass grafts are characterized by minor calcification compared to naive vessels, allowing more accurate analysis in most cases. Coronary calcifications and metal clip artifacts still remain a challenging issue with 64-slice cardiac CT despite improvements with the use of sharper image filters, e.g. the B46 Kernel (Siemens Medical Solutions) (Seifarth et al., 2005). The another important limitation is the high radiation dose required for 64-slice MDCT, although electrocardiogram-dependent dose modulation can reduce this by 30%–50%. The minimization of radiation exposure as well as optimization of the diagnostic accuracy in calcified vessels remain the chief goals for future MDCT advances.

2.3. Strategies for reduction of radiation dose and image noise

Current limitations of coronary CTA include image noise and radiation dose. As a result, a number of techniques and strategies have become available on newer CT platforms to enable dose reduction in coronary CT. These include sequential or prospective ECG triggering, reduced tube voltage scanning, and high-pitch helical scanning. Recently, iterative reconstruction (Adaptive Statistical Iterative Reconstruction [ASIR], GE Healthcare) has been introduced as a new reconstruction algorithm (Rajiah et al., 2012; Leipsic et al., 2007; Min et al., 2009). In comparison with filtered back projection (FBP), ASIR reduces image noise (increase contrast-to-noise ratio [CNR]) by iteratively comparing the acquired image to a modeled projection. This reconstruction algorithm is used to help deal with one of the primary issues of dose and tube current reduction for coronary CTA with FBP: increased image noise with decreased tube current. Recently, a high-definition CT (HDCT) scanner, with improved in-

http://dx.doi.org/10.5772/54085

plane spatial resolution of 230 μm and the ability to reconstruct images with the use of a novel applied ASIR algorithm, has been developed (Min et al., 2009).

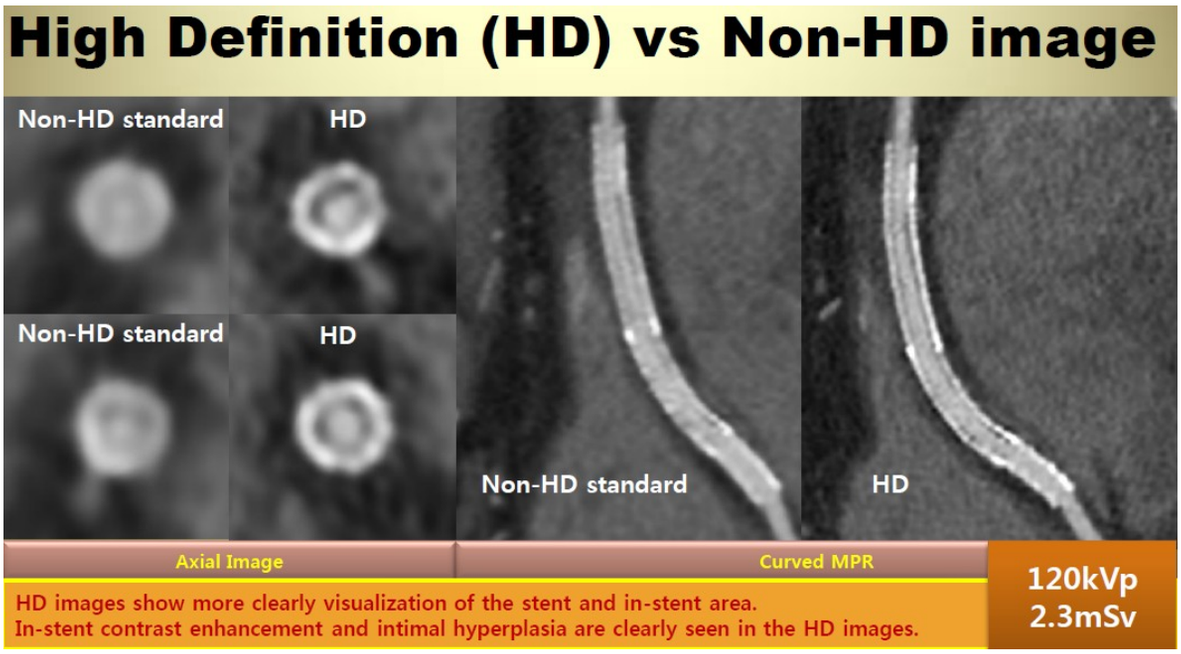

Scheme 1. High definition (HD) versus non-HD CT imagings. HD images show more clearly visualization of the stent and in-stent area.

3. Coronary artery stent imaging with MDCT

Coronary artery stenting is currently the standard practice in nonsurgical myocardial revascularization. However, coronary in-stent restenosis attributable to intimal hyperplasia remains problematic, with an incidence rate of 20% to 30%. The evaluation of stent patency is a major issue in the follow-up after stent placement. It would be desirable to obviate the use of invasive and costly angiography in the evaluation of stent patency. Initial studies using 4-detector coronary CTA for the evaluation of stent patency showed difficulties in imaging small and high-attenuating structures such as coronary stents (Table 1). With 16-detector coronary CTA, coronary artery stent patency has been assessed on the basis of contrast enhancement measurements or pixel count methods. However, stent diameter (≤ 3 mm), strut thickness, and stent material are still a cause of poor lumen visualization. In a study by Gilard et al, 232 stents were evaluated in vivo with 16-detector CT. Lumen interpretability depended on stent diameter: for stents with diameter > 3mm, 81% of lumens were interpretable, compared with 51% for stents with diameter ≤ 3 mm (Gilard et al., 2006). Restenosis detection depended on stent diameter: for stents with diameter > 3 mm, sensitivity and specificity of MDCT were 86% and 100%, respectively. For small stents with diameter ≤ 3 mm, corresponding values were 54% and 100% (Lefebvre et al., 2007; Pugliese et al., 2006). As stated by Kitagawa et al, the importance of metal artifacts and partial volume effect of stents is related to the stent material, the stent diameter and thickness, and the strut

design (Kitagawa et al., 2006). In vitro studies comparing 16-slice CT with 4-slice CT showed improvement in lumen visibility, with the same medium smooth body kernel (B30f) for reconstruction (Maintz et al., 2003). The use of a dedicated high spatial resolution reconstruction kernel (sharp kernel or "B46f"), compared with a standard reconstruction kernel (medium-smooth kernel or "B30f"), resulted in a further improvement of the visible stent lumen diameter because, with the B46f-kernel, the stent boundary was depicted more sharply than on the B30f-kernel images. Further, a larger window width to suppress the high attenuation of the stent strut seemed to contribute better delineation and more accurate measurement of the in-stent lumen. In a phantom study, Seifarth et al. showed that the use of 64-slice CT results in superior visualization of the stent lumen and in-stent stenosis, compared with 16-slice CT (Seifarth et al., 2006). In addition to evaluating the in vitro and in vivo performance of 64-slice CT for stent analysis, further developments could focus on the design of stents to reduce artifacts.

Authors	CT technique	Number of Patients	Number of Stents	Stent Caliber (mm)	Criteria for patency	Sensitivity (%)	Specificity (%)
Pump, et al., 2000	Electron beam	202	321	-	Distal runoff	78	98
Knollman, et al., 2004	Electron beam	117	152	2.5- 3.0	Distal runoff	72	60
Maintz, et al., 2003	4-MDCT	29	47	3.0-5.0	Distal runoff	100	100
Ligabue, et al., 2004	4-MDCT	48	72	2.5-4.5	Distal runoff	100	100
Schuijf, et al., 2004	16-MDCT	22	68	2.25-5.0	Distal runoff	78	100
Gilard, et al., 2006	16-MDCT	143	232	2.5-4.5	visualize lumen	100	92

Table 1. Results of studies of the use of MDCT to evaluate coronary stent patency.

3.1. Beam hardening and blooming effect

Metallic struts cause a severe CT artifact known as blooming effect. Blooming effect results from beam hardening and causes the stent struts to appear thicker than they are and, often, to overlap the vessel lumen. As a result the in-stent luminal diameter is underestimated. The energy spectrum of the x-ray beam increases as it passes through a hyperattenuating structure because lower-energy photons are absorbed more rapidly than are higher-energy photons, resulting in the beam being more intense when it reaches the detectors. Calcified spots of vessel wall near or at the outer surface of an implanted stent also contribute to beam hardening, which further erodes the assessability of the stent lumen. Depending on the metal type and the design of the stent, the magnitude of this artifact varies. As a rule, the depiction of stents with the slimmest profile is least affected by blooming artifacts (Lefebvre et al., 2007; Pugliese et al., 2006).

http://dx.doi.org/10.5772/54085

3.2. Partial volume averaging and interpolation

Another obstacle to coronary stent imaging is related to partial volume averaging and interpolation. Inherent in all digital tomographic imaging techniques, partial volume averaging yields a CT number that represents average attenuation of the materials within a voxel. At stent imaging in vessels with a large diameter, such as the aorta or iliac arteries, partial volume averaging effects are present but are limited to the proximity of the vessel wall. In coronary arteries with smaller diameters, the artifacts are of the same magnitude, but a reliable assessment of the lumen is much more problematic. The smaller the stent, the more detrimental the effect of partial volume averaging on the assessability of the in-stent lumen. The thinner detector width on 64-section CT scanners partly solves this problem by reducing the voxel size and thereby the general assessability of the stent lumen (Lefebvre et al., 2007; Pugliese et al., 2006).

3.3. Stent type

The visibility of lumens of different stents varies and this largely depends upon the stent type and the diameter. The blooming effect is more disturbing for smaller coronary stents with thicker struts. Uninterpretable images tend to be obtained for stents with thicker struts and/or a smaller diameter. When the lumen diameter is less than 3mm, the lumen visibility is worse. Regarding the type of stent, the most severe artifacts are found with tantalum, gold or gold-coated stents, or with covered stent grafts as compared with stainless steel stents. Maintz et al. recently evaluated 68 different stents in vitro with using 64-slice MDCT and they created a catalogue of the CT appearance of most of the currently available coronary stents (Maintz et al., 2009). They confirmed that the high variability for stent lumen visibility depended on the stent type, and this was previously reported on with using 4-slice and 16-slice CT. They also concluded that while in vivo studies will be required to verify their results, it can be assumed that a reliable evaluation of lumens of stents in the more advantageous stent types, such as the Radius, Teneo, Symbiot or Flex standard stents, will be possible with using 64-slice MDCT. First-generation drug-eluting stents, which released sirolimus or paclitaxel, were shown to be superior to bare-metal stents and to balloon angioplasty in reducing the magnitude of neointimal proliferation, the incidence of clinical restenosis, and the need for reintervention. Unfortunately, late stent thrombosis (thrombosis that occurs 30 days or more after implantation of the stent) is more likely to occur with drug-eluting stents than with bare-metal stents. The gradual release of the antiproliferative agent effectively inhibits endothelialization of the stent struts, thereby allowing them to continue to serve as a nidus for platelet aggregation and thrombus formation. Second or third-generation drug-eluting stents are designed to provide better stent deployment, safety, and efficacy. They differ from the first-generation stents with respect to the antiproliferative agent, the polymer layer (which acts as a reservoir for controlled drug delivery), and the stent frame. Improvements in stent structure may result in better stent apposition to the vessel wall, improved endothelialization (a thin stent strut elicits less neointimal proliferation and requires less endothelialization to cover the struts completely), and reduced platelet aggregation and thrombus formation, thereby reducing the incidence of stent thrombosis.

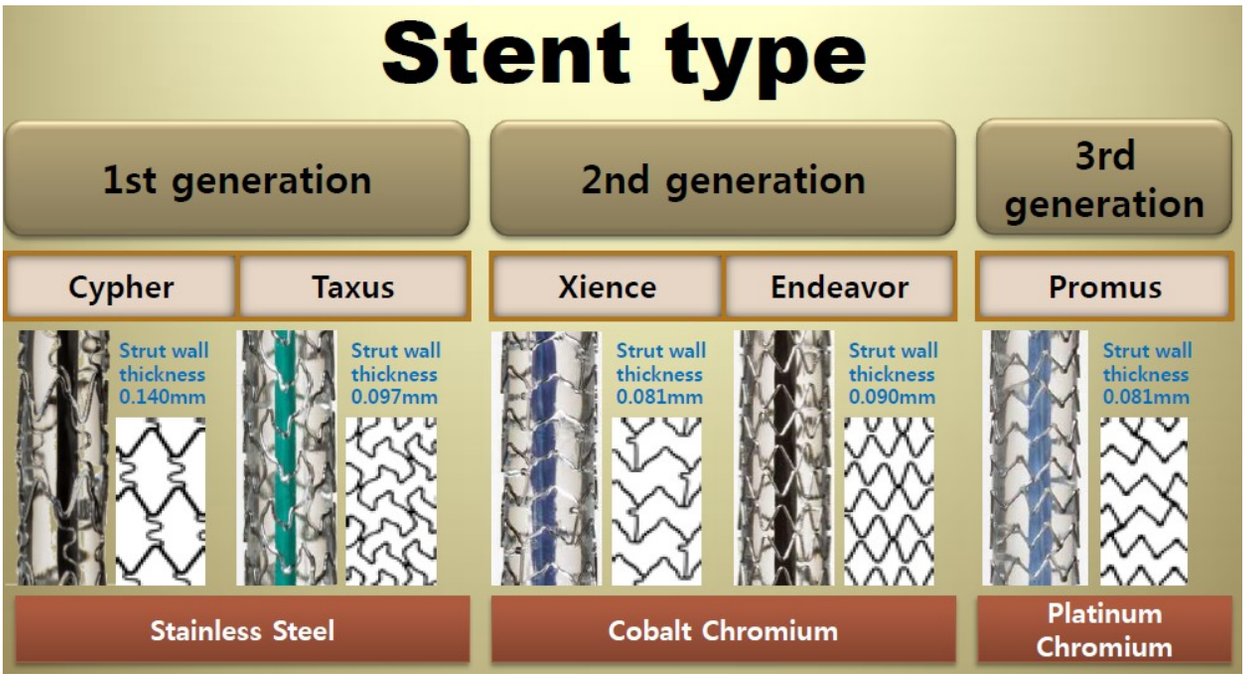

Scheme 2. Detail render of drug-eluting stents. Diverse drug-eluting stents are currently available, differing in the type of metal used, stent design, and drug coating.

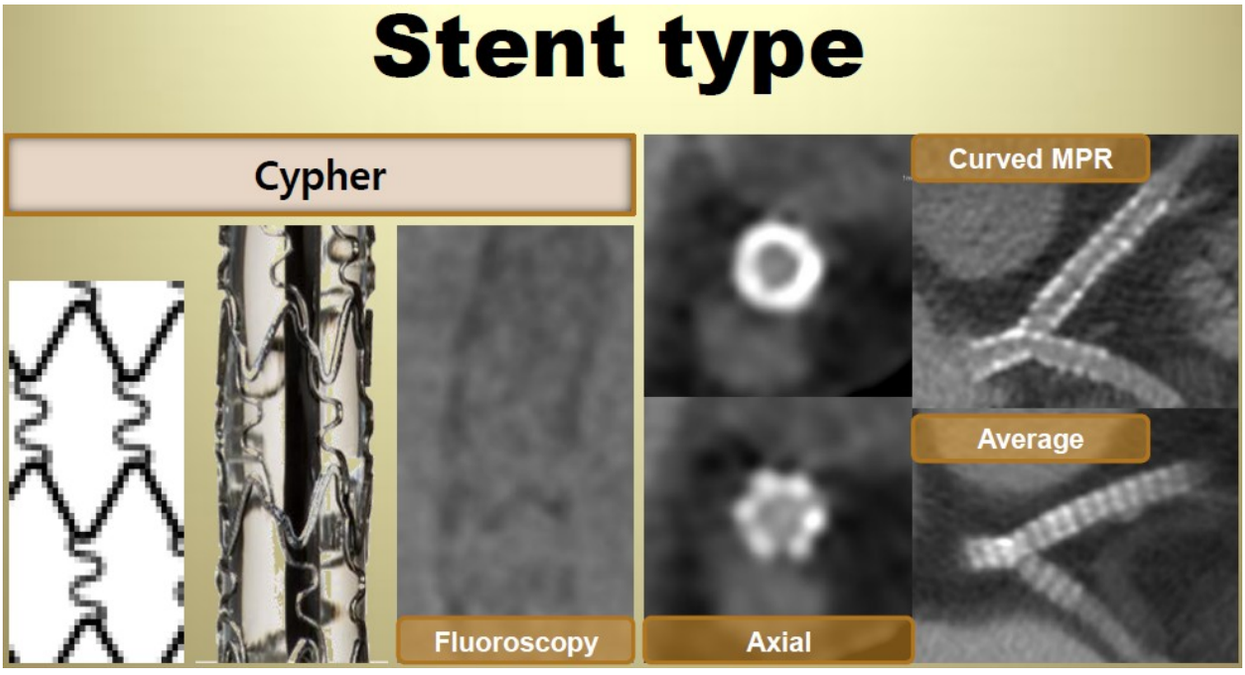

Scheme 3. Type of metal used, stent design, and images of fluoroscopy and 64-slice MDCT of Cypher, first-generation Sirolimus-eluting stent.

http://dx.doi.org/10.5772/54085

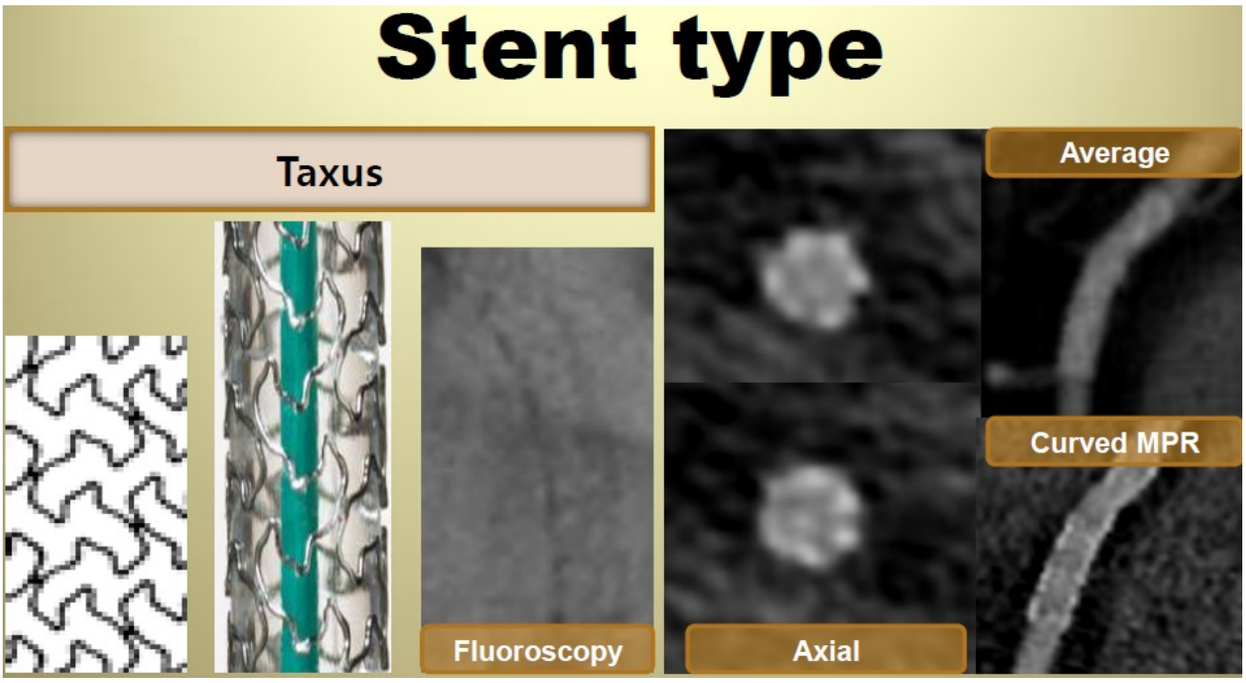

Scheme 4. Type of metal used, stent design, and images of fluoroscopy and 64-slice MDCT of Taxus, first-generation Paclitaxel-eluting stent.

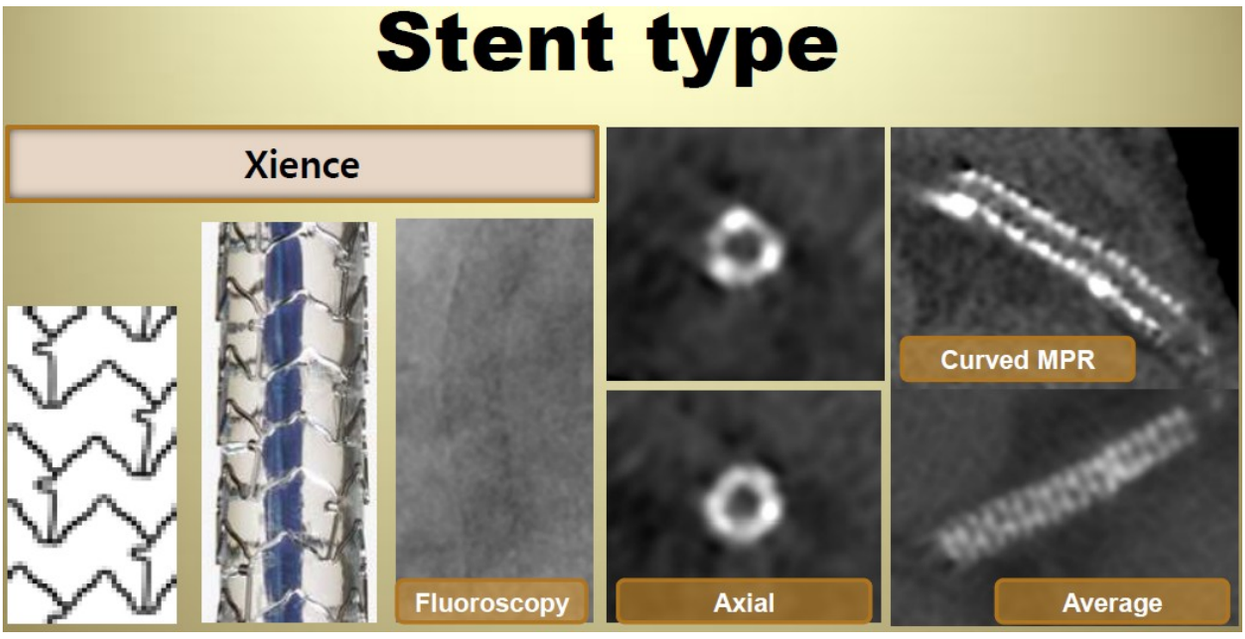

Scheme 5. Type of metal used, stent design, and images of fluoroscopy and 64-slice MDCT of Xience, second-generation Everolimus-eluting stent.

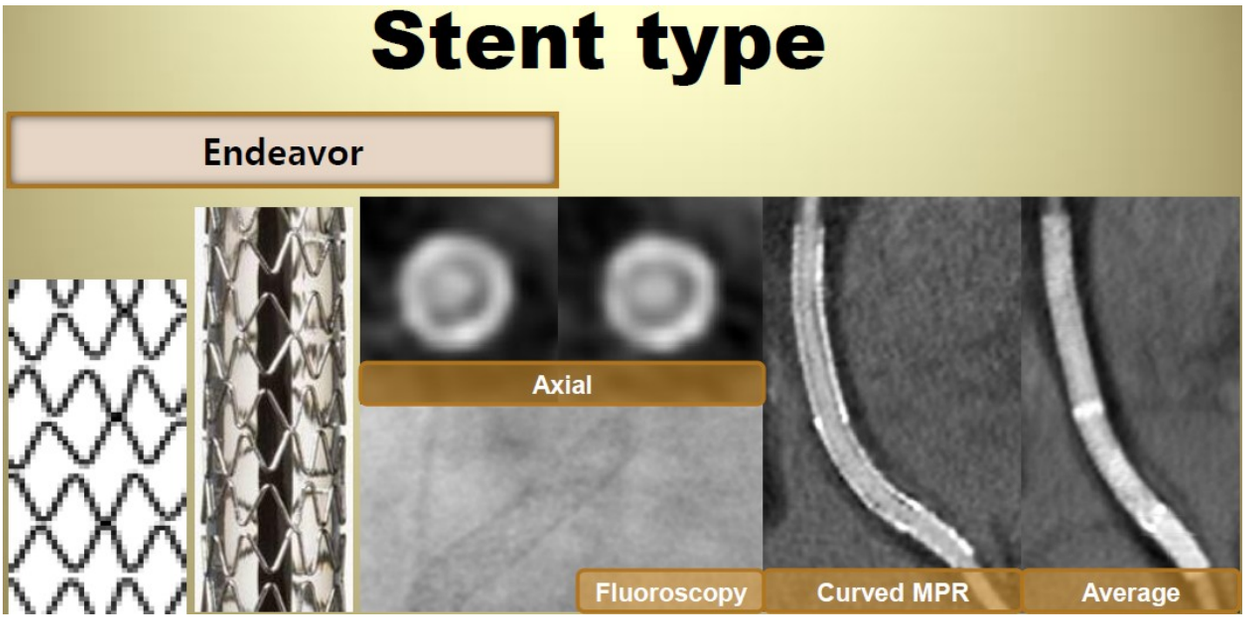

Scheme 6. Type of metal used, stent design, and images of fluoroscopy and 64-slice MDCT of Endeavor, second-generation Zotarolimus-eluting stent.

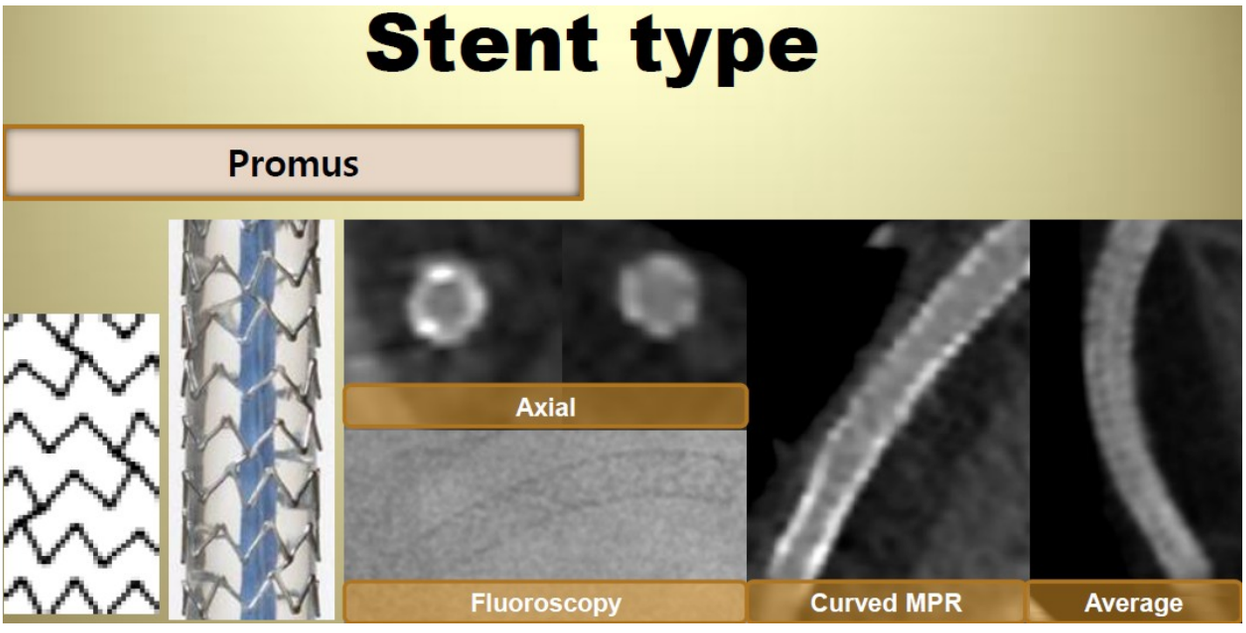

Scheme 7. Type of metal used, stent design, and images of fluoroscopy and 64-slice MDCT of Promus, third-generation Everolimus-eluting stent.

http://dx.doi.org/10.5772/54085

Stent trade name	Metal platform	Coating drug used
Cypher	Stainless steel	Sirolimus (Rapamune)
Endeavor	Cobalt-chromium	Zotarolimus
Taxus	Stainless steel	Paclitaxel (Taxol)
Xience, Promus	Cobalt-chromium	Everolimus (Afinitor)

Table 2. Types of Drug-Eluting Stents Available for Clinical Use

3.4. Optimization of contrast enhancement

Prominent contrast enhancement in the lumen is a prerequisite for robust coronary CT angiography. It is achieved not only by optimizing the contrast material injection parameters (example, using a high-concentration contrast agent and a fast injection rate) but also by accurately synchronizing CT data acquisition with the passage of the contrast agent by means of bolus tracking or a test bolus. Edge-enhancing convolution filters, which may be used for better delineation of stents, have the drawback of producing noisier data sets. If such convolution filter is used, the assessability of in-stent lumen particularly benefits from the presence of high degree of intraluminal contrast enhancement, which somewhat compensates for the kernel-related noise. A high degree of intraluminal enhancement is recommended especially for the investigation of stent patency in vessels that have a small diameter and thus contain less blood (Lefebvre et al., 2007; Pugliese et al., 2006).

3.5. Residual cardiac motion

Residual cardiac motion is of the utmost importance as a cause of vessel non-assessability at MDCT. Residual cardiac motion also plays a role in exacerbating metal-related artifacts such as beam hardening or partial volume averaging effects. The use of high gantry rotation speeds, multisegmental reconstruction techniques, and beta-blockers to lower the heart rate consistently improves the interpretability of MDCT. ECG-based editing techniques allow improvement of image quality for patients with mild irregularities in sinus rhythm, such as premature beats, and for those with bundle-branch block (Lefebvre et al., 2007; Pugliese et al., 2006).

3.6. In-stent lumen evaluation

As mentioned earlier, the direct visualization of the in-stent lumen is important for assessing patency, because collateral vessels may be feeding vessel segment distal to the occluded stent in a retrograde direction. An accurate intraluminal evaluation can best be performed by means of multiplanar reformation of the CT data volume. The stent may be considered to be occluded if the lumen inside the device appears darker than the contrast-enhanced vessel lumen proximal to the stent. Unless severe artifacts affect the CT data set, stent evaluation may proceed beyond a judgment of patency or occlusion. Nonocclusive in-stent neointimal hyperplasia is characterized by the presence of a darker rim between the stent and the contrast-enhanced vessel lumen and is secondary to the healing response to procedurerelated

vessel injury. If neointimal hyperplasia exceeds a luminal diameter reduction of 50%, the process is consistent with hemodynamically significant in-stent restenosis. Instent restenosis typically occurs as a localized nonenhancing lesion, often (but not invariably) associated with complex lesion anatomy and discontinuity in lesion coverage. Restenosis may occur either within or adjacent to the stent (within 5 mm of the stent extremities). Edge restenosis might occur because of a decrease in local drug availability, incomplete lesion coverage due to a gap between two stents, procedure-related trauma, or damage to the polymer coating of a stent from calcifications or an overlapping stent.

3.7. Coronary stent fracture

Stent fracture (SF) is an important and potentially serious complication of drug-eluting stents (DES), resulting in thrombosis and in-stent restenosis. Recent reports suggest that the prevalence of fracture ranges between 1.9% and 2.6% (Dimitrios et al., 2011; Lim et al., 2008). SF is probably related to mechanical fatigue of the metallic stent strut, which may be aggravated by highly pulsatile structures such as myocardial bridge, use of long stents or DES unsupported by neointimal tissue. SF may also result from a manufacturing defect. Various factors that have been implicated for a stent fracture include vessel tortuosity, the presence of a right coronary artery lesion, overlapping stents, and the use of a DES such as a sirolimus-eluting stent. In general stent fractures have been reported to be more common when placed in the right coronary artery (RCA) probably due to its curved course, than in the left anterior descending (LAD) or circumflex (LCX) coronary arteries. The type of stent also influences its risk for fracture. The Cypher stent is more prone to fracture as compared to Taxus and Endeavor stents. Overlapping stents are more likely to fracture rather than isolated stents. The presence of stent fracture was classified as grade I to V: I = involving a single-strut fracture; II = 2 or more strut fractures without deformation; III = 2 or more strut fractures with deformation; IV = multiple strut fractures with acquired transection but without gap; and V = multiple strut fractures with acquired transection with gap in the stent body (Nakazawa et al., 2009).

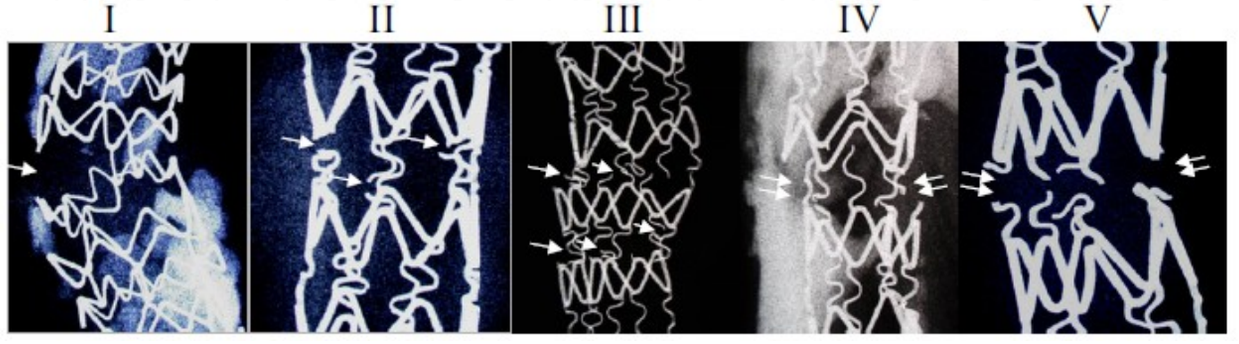

Scheme 8. Classification of stent fracture.

http://dx.doi.org/10.5772/54085

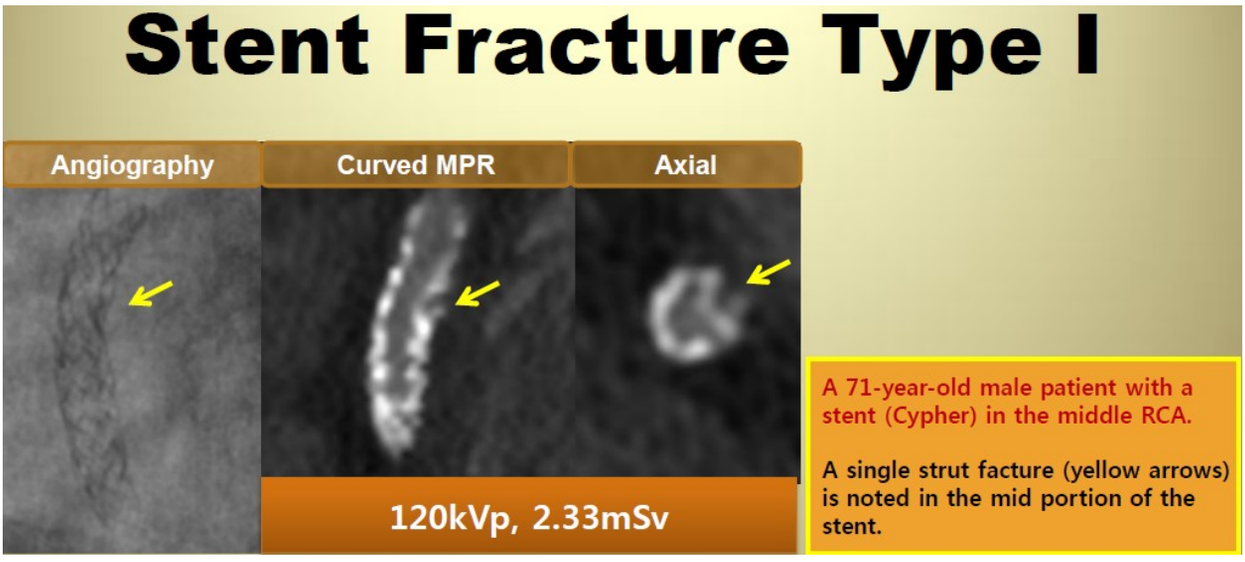

Scheme 9. Images of fluoroscopy and 64-slice MDCT of stent fracture type I. A single strut fracture is seen in the mid portion of the stent in RCA.

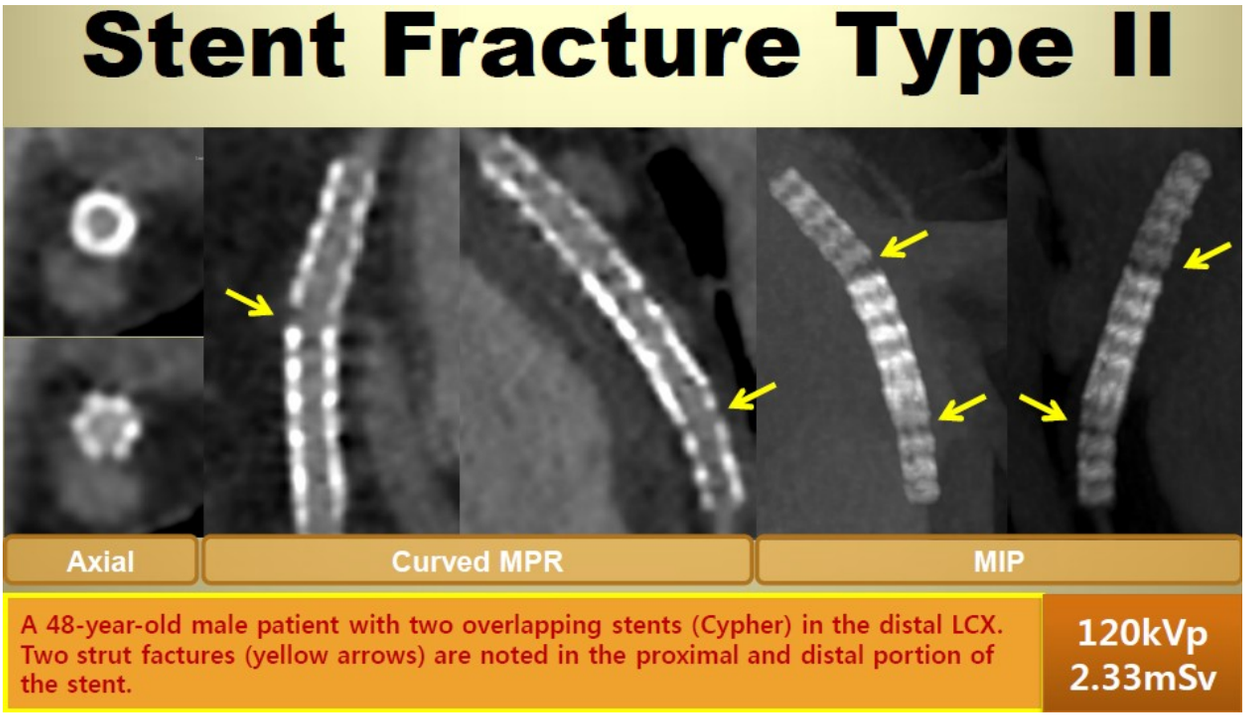

Scheme 10. Images of fluoroscopy and 64-slice MDCT of stent fracture type II. Two strut fractures are seen in the proximal and distal portion of the stent in LCX.

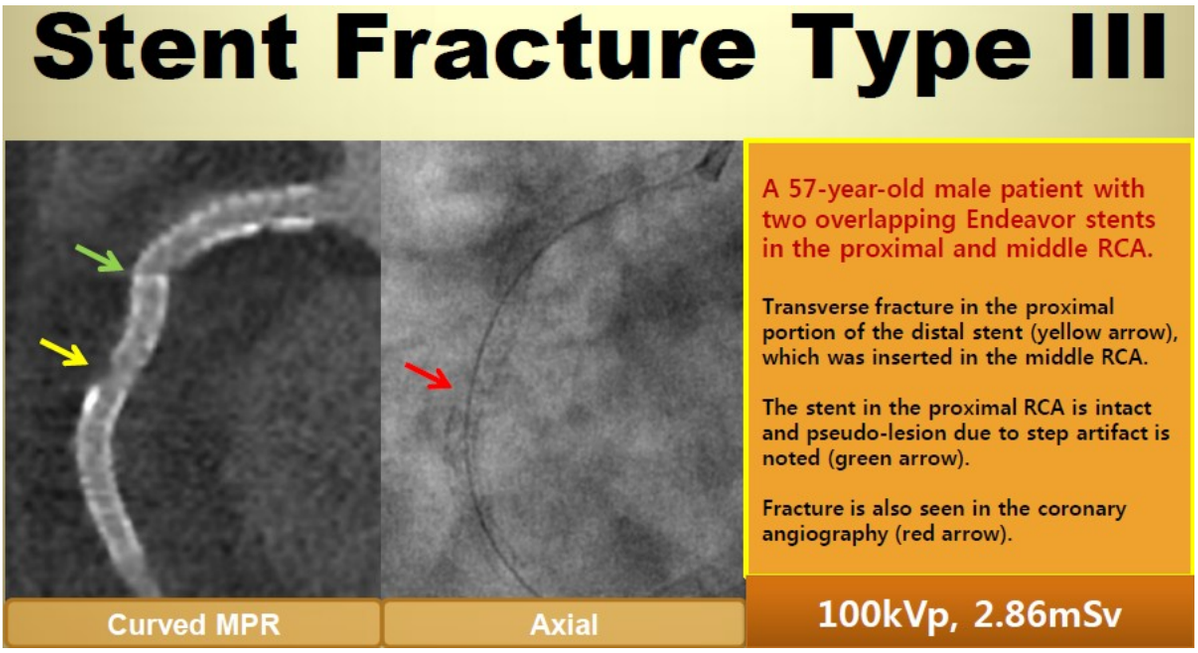

Scheme 11. Images of fluoroscopy and 64-slice MDCT of stent fracture type III. Transverse fracture with deformation is seen in the proximal portion of the stent in middle RCA. The stent in proximal RCA is intact in coronary angiography suggesting pseudo-lesion due to step artifact in MDCT.

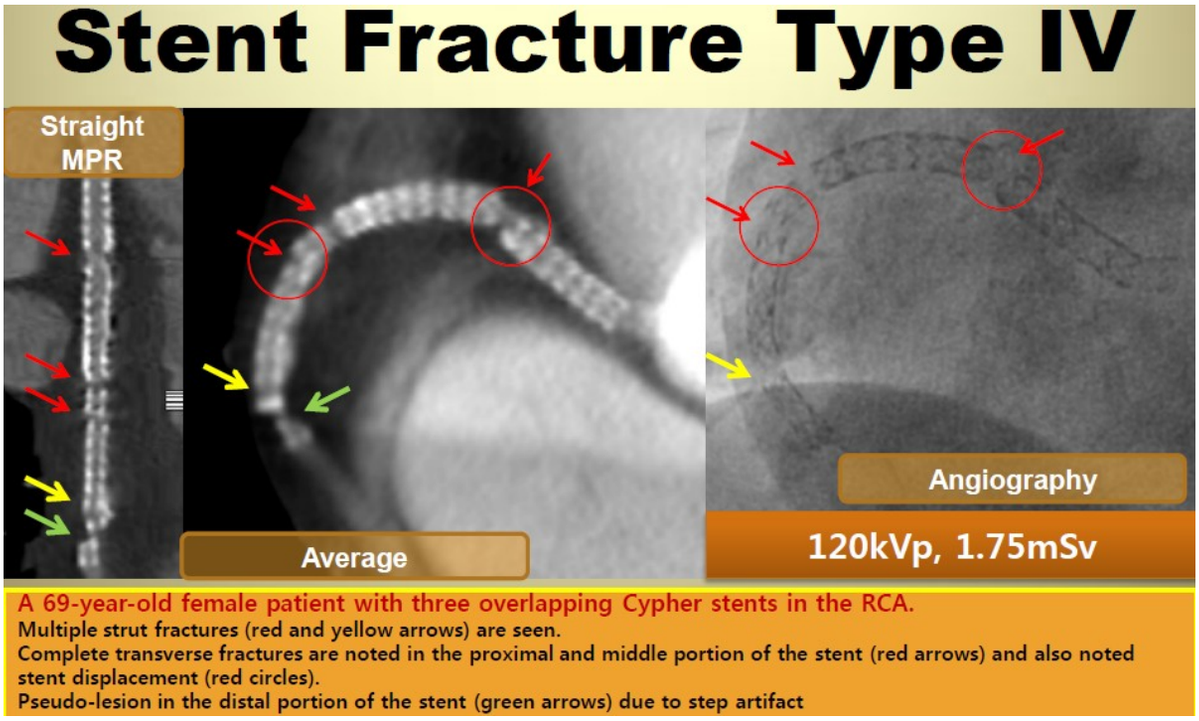

Scheme 12. Images of fluoroscopy and 64-slice MDCT of stent fracture type IV. Multiple strut fractures with acquired transection without gap are seen in the proximal and mid portion of the stent in RCA. The distal portion of the stent is intact in coronary angiography suggesting pseudo-lesion due to step artifact in MDCT.

http://dx.doi.org/10.5772/54085

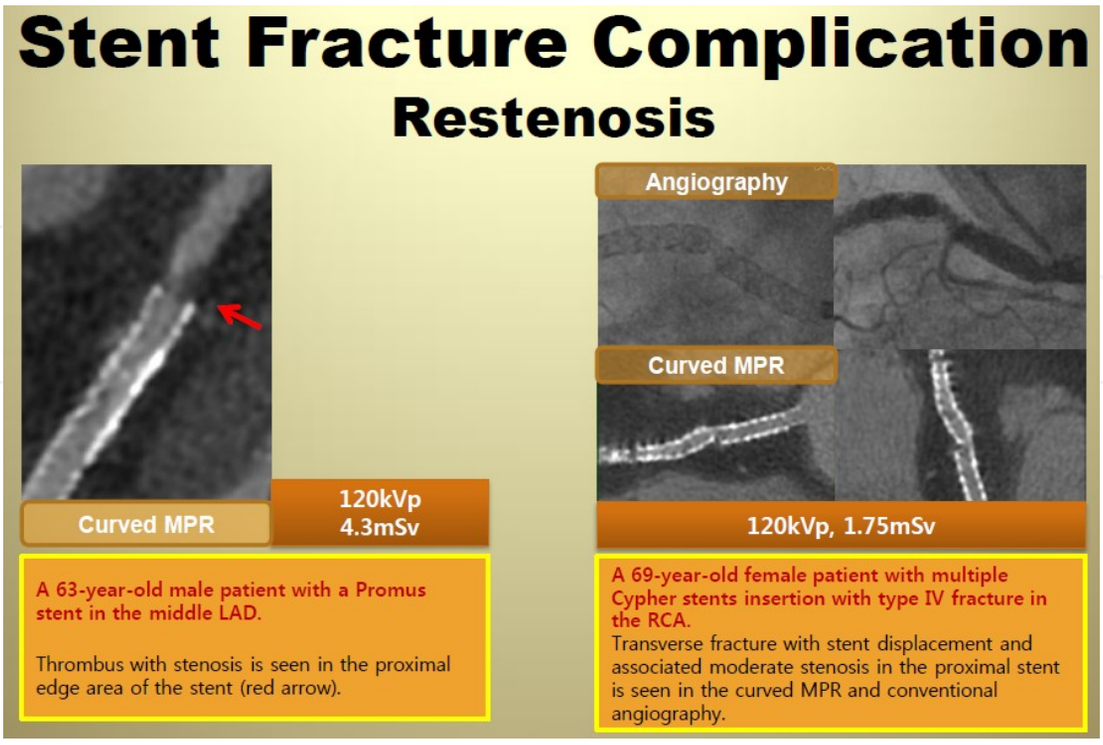

Scheme 13. Images of fluoroscopy and 64-slice MDCT of restenosis due to stent fracture. (Left) Thrombus with stenosis is seen in the proximal edge of the LAD stent. (Right) Transverse fracture with stent displacement and moderate stenosis is seen in the RCA stent.

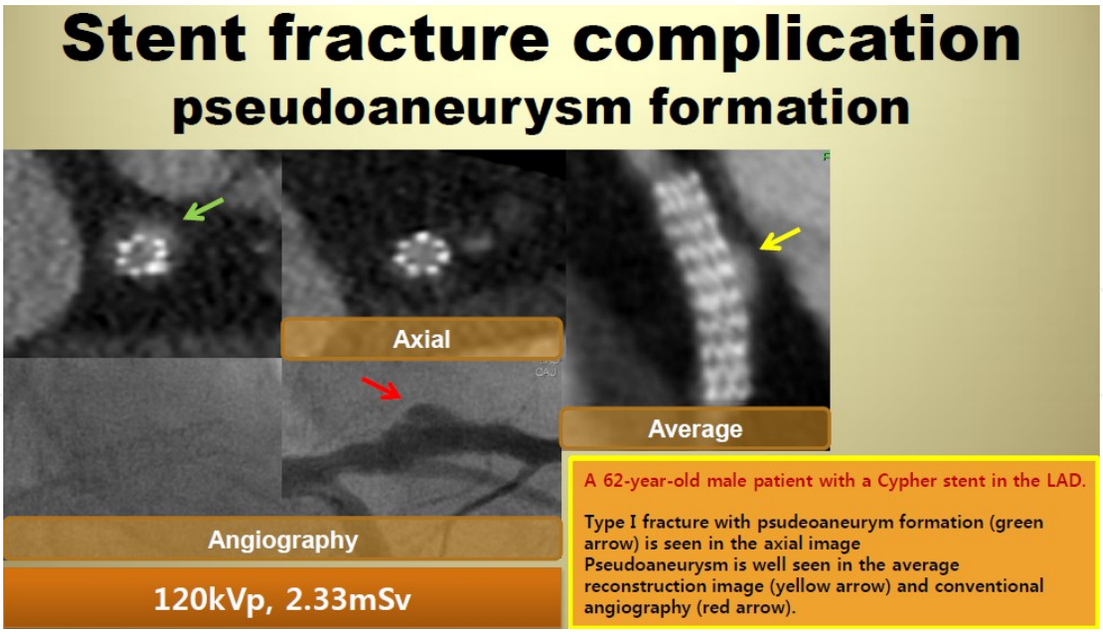

Scheme 14. Images of fluoroscopy and 64-slice MDCT of pseudoaneurysm due to stent fracture. Type I fracture with pseudoaneurysm formation is seen in the LAD stent.

SF has been evaluated mainly by using conventional coronary angiography or fluoroscopy and in selected cases by intravascular ultrasound (IVUS). Recently, MDCT has been found to be more sensitive than conventional coronary angiography in the detection of SF, due to its nearly isotropic multi-planar imaging capabilities, that can depict stents in their long and short axes (Lim et al., 2008; Pang et al., 2009). MDCT imaging on 64-slice scanners provide most of the relevant details required to assess stents on follow-up. In a retrospective evaluation, 64-slice MDCT angiography of 371 patients with 545 stents identified 24 SFs, of which 6 were not detected on conventional angiograms at the initial readings (Lim et al., 2008). An *in vitro* comparison of 64-slice MDCT, conventional cine-angiography, and IVUS revealed that MDCT had high accuracy for the evaluation of coronary SF (Pang et al., 2009). The important features that must be evaluated in all post-stent follow-up include not only the evaluation of in-stent thrombosis, but also features such as stent migration, fracture, buckling, and rarely coronary perforation and aneurysms or pseudoaneurysms (Dimitrios et al., 2011).

4. Coronary artery bypass graft imaging with MDCT

4.1. Coronary bypass graft lumen assessment: Graft patency and stenoses

Coronary bypass graft CT can be performed with 2 different objectives, each with a separate clinical context and goal: the evaluation of graft patency, and the evaluation of graft and anastomotic stenoses. Within the first postoperative month, the main cause of graft failure is thrombosis.75 Graft closure from thrombosis at 1 month is a known complication in 10% to 15% of cases. Coronary bypass graft patency assessment has been shown to be excellent with ECG-gated 4-detector CT, with mean sensibility and specificity for occlusion of 97% and 98%, respectively, in comparison with catheter angiography (Nieman K et al., 2003; Marano R et al., 2004). With 16-detector CT, accuracy is also excellent, with mean sensitivity of 100 % and mean specificity of 99% for detecting bypass graft occlusion, in comparison with catheter angiography (Chiurlia E et al., 2005; Anderson K et al., 2006). Recent studies using 64-slice MDCT have reported sensitivity and specificity values of 95% to 100% and 93% to 100%, respectively, for graft occlusion and high-grade stenosis with > 50% luminal narrowing. Since naïve coronary arteries and coronary grafts are small vessels, 2 to 4 mm in diameter, and are characterized by both complex anatomy and continuous movements, high spatial and temporal resolutions are mandatory to visualize these vessels at MDCT. Vascular clips in the proximity of grafts and their anastomoses, as well as artifacts owing to residual cardiac motion, can be a cause of significant artifacts for the evaluation of graft stenoses.

4.2. Type of arterial or vein graft

4.2.1. Saphenous vein Graft (SVG)

The SVG was first successfully used in a CABG operation by Sabiston in 1962. Both the benefits and limitations of SVG have been well documented in the literature (Bourassa et

http://dx.doi.org/10.5772/54085

al., 1985; Campeau et al., 1983). Saphenousveins are fairly simple to access and harvest from the lower extremities, and they are more versatile and widely available than arterial grafts. In addition, during the intra- and perioperative period, saphenous veins are resistant to spasm versus their arterial counterparts. However, the use of SVG is limited by distortion from varicose and sclerotic disease as well as a higher occurrence of intimal hyperplasia and atherosclerotic changes after exposure to systemic blood pressure, resulting in lower patency rates. Graft occlusion can also occur due to vascular damage during harvesting of the saphenous vein. In a large study, the SVG patency was 88% perioperatively, 81% at 1 year, 75% at 5 years, and 50% at greater than or equal to 15 years (Fitzgibbon et al., 1996). The graft attrition rate between 1 and 6 years after CABG surgery is 1% to 2% per year, and between 6 and 10 years is 4% per year. The great saphenous vein is the vein routinely used for CABG surgery. The proximal anastomosis of the venous graft with the ascending aorta is usually performed cranial to the origin of coronary arteries and as distal as the proximal portion of the aortic arch. The SVG can be sutured directly to the anterior portion of the ascending aorta or attached with an anastomotic device, allowing faster, sutureless attachment. The device, called the Symmetry Bypass System aortic connector (St Jude Medical, St Paul, Minn), alters the common appearance of the bypass graft by requiring the aortic connector to be anastomosed perpendicularly to the aorta (Mack et al., 2003; Poston et al., 2004). Recent reports have documented the development of significant stenosis and occlusion in 13.7%-15.5% of vein grafts attached with the aortic connector (Carrel et al., 2003; Wiklund et al., 2002). In order to support the course of the aortovenous anastomosis, the left-sided SVG is connected to the left side of the aorta, stabilizing the graft on top of the main pulmonary artery. A right-sided SVG is attached either to the lower aspect or right side of the ascending aorta, allowing the graft to traverse the right arterio-ventricular groove. SVGs tend to appear as large contrast-filled vessels (Fig.1).

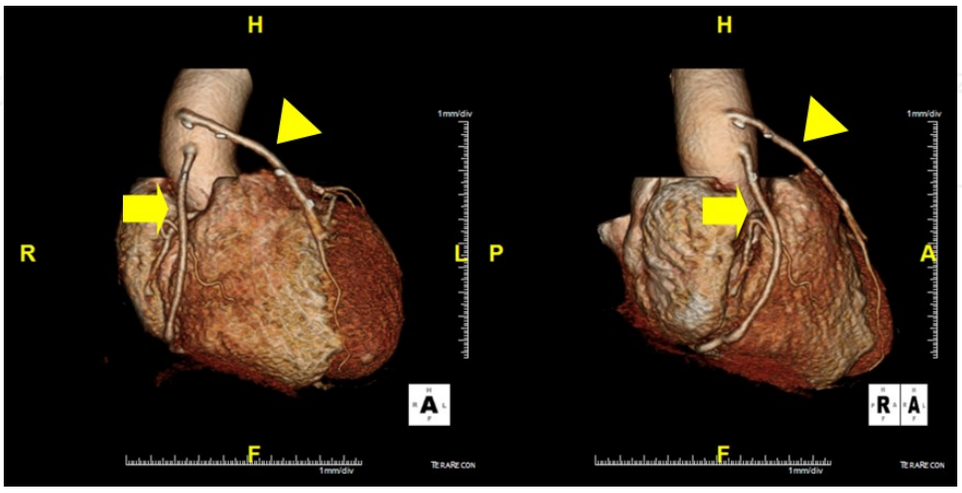

Figure 1. Saphenous vein grafts. Three-dimensional volume-rendered images show the typical appearance of right (arrow) and left (arrowhead) saphenous vein grafts (SVGs) sutured to the anterior aorta. The left SVG is attached to

the mid-portion of left anterior descending (LAD) artery and the right SVG is attached to the distal-portion of right coronary artery (RCA).

An SVG to the right side is attached to the distal right coronary artery (RCA), posterior descending artery (PDA), or distal LAD artery. The distal anastomosis may lie on the phrenic wall of the heart. An SVG to the left side is attached distally to the LAD artery, diagonal artery, left circumflex (LCx) artery, or the obtuse marginal (OM) arteries, by traversing anteriorly and superiorly to the right ventricular outflow tractor main pulmonary artery (Fig. 2, 3, 4).

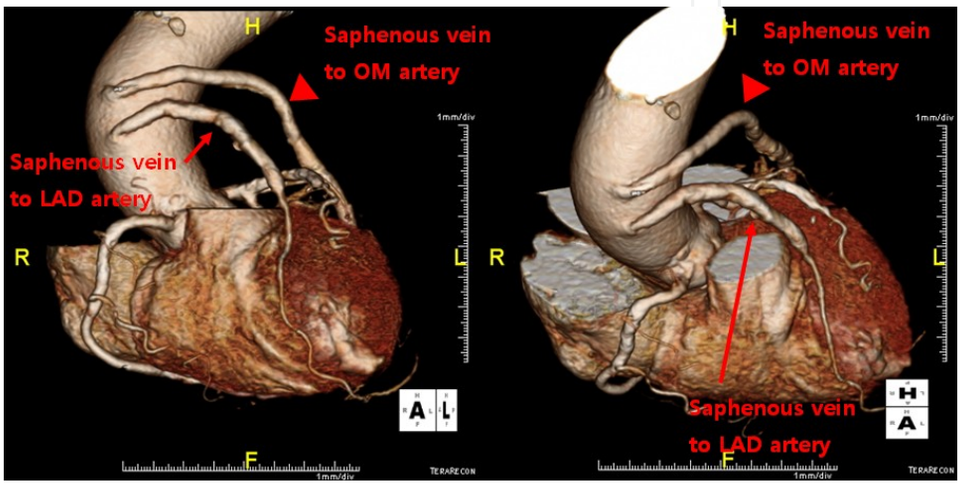

Figure 2. Saphenous vein grafts. Three-dimensional volume-rendered images show the typical appearance of right (arrow) and left (arrowhead) saphenous vein grafts (SVGs) sutured to the anterior aorta. The right SVG is attached to the mid-portion of left anterior descending (LAD) artery and the left SVG is attached to the obtuse marginal (OM) artery.

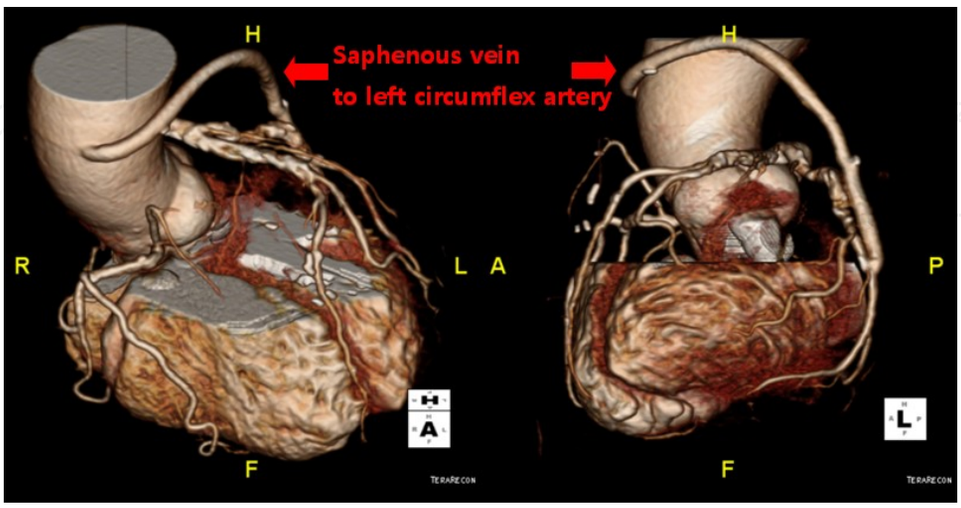

Figure 3. Saphenous vein graft. Three-dimensional volume-rendered images show the left saphenous vein graft (SVG) with its anastomosis with the left circumflex (LCx) artery.

http://dx.doi.org/10.5772/54085

SVG may present a horizontal or slightly oblique course on axial images, especially when the distal anastomosis is placed on the LCx or a diagonal branch to supply the left cardiac wall. In these cases, the graft can be recognized in the fatty tissue of mediastinum, posterior to the sternum and anterior to the RVOT. On occasion, the distal SVG is anastomosed sequentially to greater than or equal to 2 coronary vessels or in the same vessel, using side-to-side and end-to-side anastomoses. The naive vessel distal to the anastamotic site should be assessed and is recognized by its position and smaller caliber compared with the SVG (Fig. 3, 4). Typically, venous grafts are larger than arterial grafts and are not accompanied by surgical clips along their course. Sometimes a circumferential clip can be identified at the site of proximal anastomosis with the ascending aorta (Fig.1).

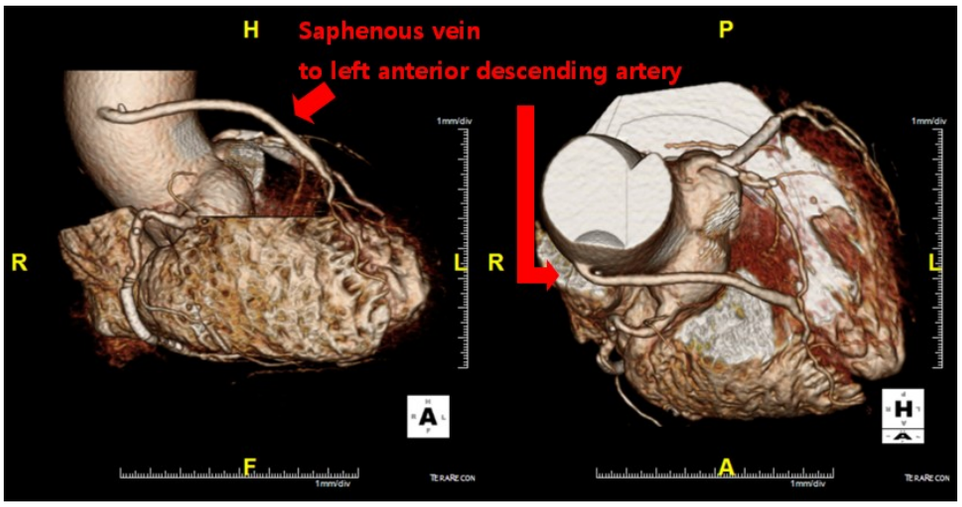

Figure 4. Saphenous vein graft. Three-dimensional volume-rendered images show the left saphenous vein graft (SVG), which is attached to the mid-portion of left anterior descending (LAD) artery.

4.2.2. Internal Mammary Artery (IMA)

The internal mammary artery (IMA) is characterized by unique resistance to atherosclerosis and extremely high long-term patency rates compared with the saphenous vein. The IMA has a nonfenestrated internal elastic laminawithout vaso vasorum inside the vessel wall, which tends to protect against cellular migration and intimal hyperplasia. Moreover, the medial layer of IMA is thin and poor of muscle cells with poor vasoreactivity. In addition, the endothelium produces vasodilator(nitric oxide) and platelet inhibitor (prostacyclin). Glycosaminoglycan and lipid compositions of IMA result in being less atherogenetic in comparison with venous grafts. Therefore, use of the IMA decreases all postoperative cardiac events and mortality, and is associated with a long-term patency rate well >90% at 10 years (Loop et al., 1986; Motwani & Topol, 1998).

4.2.3. Left IMA

The Left IMA (LIMA) is the vessel of choice for the surgical revascularization of the left anterior descending (LAD) artery for its biological and anatomical characteristiscs, being the conduit more proximal to the LAD artery and the easiest to harvest both in median sternotomy and mini-thoracotomy. Due to anatomical proximity to the LAD artery and favorable patency rates, the left IMA (LIMA) is most commonly used as an in situ graft to revascularize the LAD or diagonal artery, supplying the anterior or anterolateral cardiac wall. The LIMA extends from its origin at the subclavian artery and courses through the anterior mediastinum along the right ventricular outflow tract after being separated surgically from its original position in the left parasternalRegion (Fig. 5).

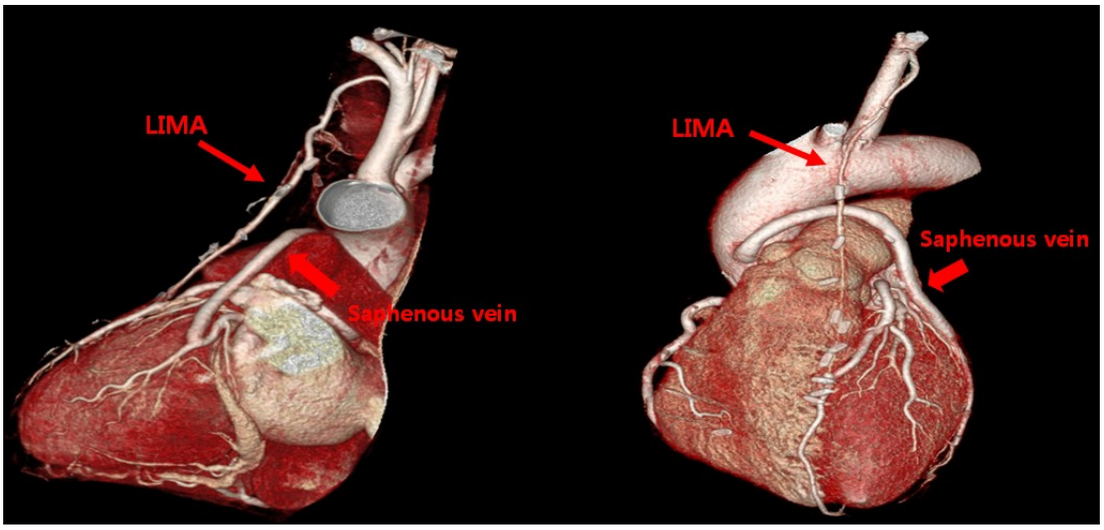

Figure 5. Left internal mammary artery (IMA) graft. Three-dimensional volume-rendered images show the left IMA graft from its origin at the left subclavian artery to its anastomosis with the left anterior descending (LAD) artery. There is also a left saphenous vein graft (SVG), which is attached to the obtuse marginal (OM) artery. Note the smaller diameter of the arterial graft compared with that of the venous graft.

Infrequently, sequential distal anastomoses, with side-to-side and end-to-side anastomoses to the diagonal and LAD arteries, respectively, or involving separate sections of the LAD artery, are performed. On axial images, the LIMA is no longer visible in its usual site, on the left side of the sternum, but courses as a small vessel in the anterior mediastinum along the right ventricle outflow tract (RVOT). Although in most cases LIMA grafts show a single distal anastomosis to the left anterior descending artery (LAD) or a diagonal branch, multiple sequential anastomoses to both the LAD and diagonal branches are sometimes performed. Surgical clips are routinely used to occlude collaterals and to avoid arterial bleeding and can be seen either adjacent to the graft or at the original site of the LIMA. As with other grafts, on CTA, the distal anastamosis is typically most difficult to visualize. Surgical clips are used routinely to occlude branch vessels of the IMA, and metallic artifact may limit assessment in some instances (Fig. 6).

http://dx.doi.org/10.5772/54085

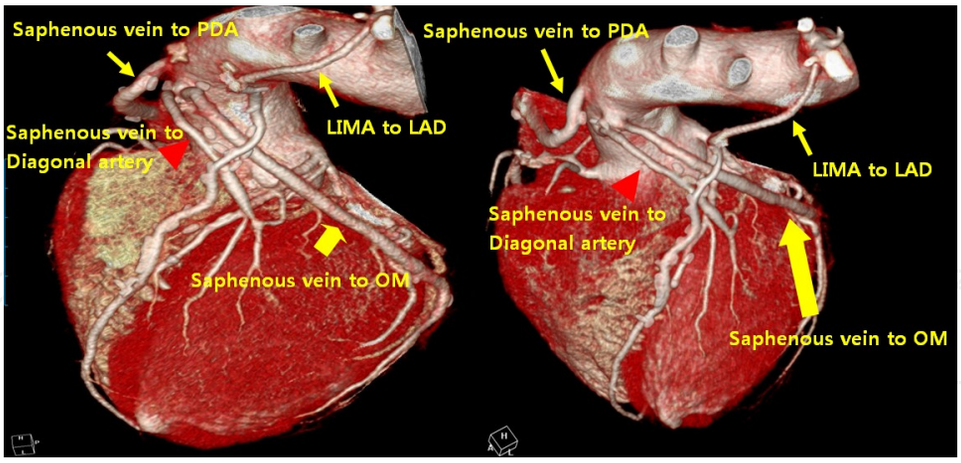

Figure 6. Left internal mammary artery (IMA) graft. Three-dimensional volume-rendered images show the left IMA graft from its origin at the left subclavian artery to its anastomosis with the left anterior descending (LAD) artery. There is also a right saphenous vein graft (SVG) sutured to the anterior aorta with its anastomosis with the posterior descending artery (PDA). The left saphenous vein grafts (SVG) are attached to diagonal artery and the obtuse marginal (OM) artery.

4.2.4. Right IMA

The right IMA (RIMA) is used less frequently than the LIMA. The RIMA may be used in a variety of ways. As an in situ graft, The RIMA remains attached to the right subclavian artery proximally and anastomoses with the target coronary artery distally. However, it is more commonly used as “free” graft from the ascending aorta to the RCA or from the LIMA to the left circumflex artery (LCx) or obtuse marginal (OM) branches. In cases in which both in situ IMAs are necessary for revascularization of the left heart, either the RIMA is connected to the LCx artery or OM branches by extension through the transverse sinus of the pericardium and the LIMA is attached to the LAD artery or the RIMA is attached to the LAD artery and the LIMA is anastomosed to the LCx artery or other side branches (OM or diagnonal branches). Otherwise, the RIMA can be removed from the right subclavian artery and used as a composite or free graft. As a segment of a composite graft to perform an arterial "T" or "Y" graft, the RIMA is anastomosed proximally to LIMA, allowing total arterial revascularization instead of using a venous graft with LIMA. As a free graft, a RIMA is anastomosed to the anterior ascending aorta and used in the same way as an SVG. The CTA appearance of the RIMA is similar to that of the LIMA. As already described for LIMA grafts, surgical clips are used to occlude collaterals. Studies have shown that total arterial myocardial revascularzation has the advantages of decreased recurrent angina and superior patency rates at 1 year when compared with those of conventional coronary artery bypass surgery in which a LIMA graft is coupled with an SVG (Muneretto et al., 2003).

4.2.5. Radial Artery (RA)

The first use of the radial artery (RA) as arterial conduit for coronary revascularization has been de-scribed by Carpentier et al in 1971 (Carpentier et al., 1973). As a muscular

artery from the forearm, the RA has a prominent medial layer and elevated vasoreactivity, which results in a lower patency rate than that of IMA grafts (Possati et al., 2003). The RA is usually harvested from the nondominant arm and is used as a third arterial graft, either as a free or composite graft or to avoid using a venous graft in case of unavailability of IMA grafts. The RA is often grafted to supply the left cardiac wall (LCx, OM). On CTA, the caliber of the RA is similar to the IMA, but it typically is visualized coursing from the ascending aorta to the naïve coronary artery (Fig. 7). In the early postoperative period, the RA may be reduced in caliber and may be difficult to identify because of vasospasm. In addition, because the RA is a muscular artery, the number of surgical clips used to close collaterals along the graft is usually higher than with IMA. This may represent a limit for noninvasive assessment of RA grafts with MDCT because of artifacts from surgical clips limiting a full CTA evaluation of an RA graft.

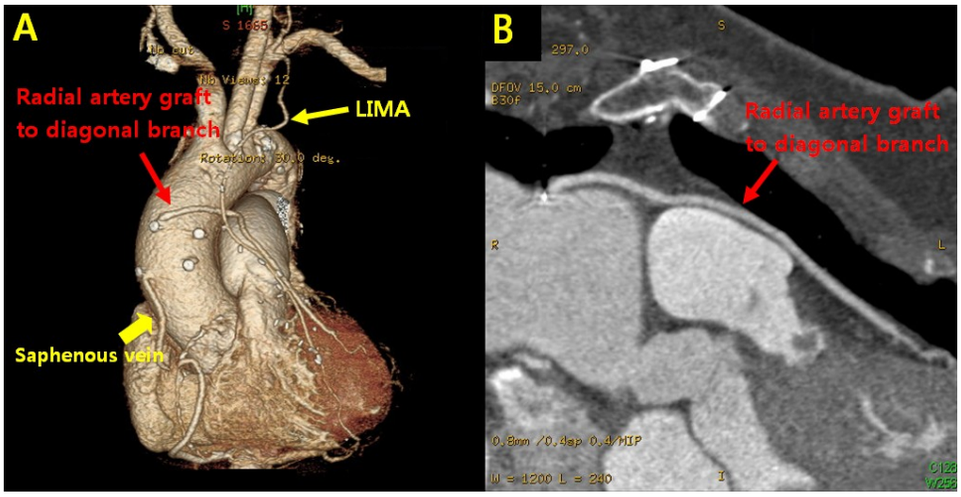

Figure 7. Radial artery (RA) graft. (A) Three-dimensional volume-rendered image shows radial artery graft sutured to the anterior aorta with its anastomosis with diagonal artery. There are also left internal mammary artery (LIMA) graft from its origin at the left subclavian artery to its anastomosis with the left anterior descending (LAD) artery and right saphenous vein graft (SVG), which is attached to the distal right coronary artery (RCA). Note the diameter of the RA is similar to the IMA, but it typically is visualized coursing from the ascending aorta to the diagonal artery. (B) Curved multiplanar reformation image shows patent RA graft within the anterior mediastinum. The full extent of the graft is seen from the ascending aorta to diagonal artery.

4.2.6. Right gastroepiploic artery (RGEA) and inferior epigastric artery (IEA)

The use of right gastroepiploic and inferior epigastric arteries in CABG procedures has been limited because of the need to extend the median sternotomy to expose the abdominal cavity (Buche et al., 1992; Manapat et al., 1994; Pym et al., 1987). Although the use of these arteries increases surgical time and technical difficulty of the surgery, these arteries can be used as a free graft to perform total arterial revascularization. The use of the RGEA was first described by Pym et al in June 1984 (Pym et al., 1987). Although it has been originally used in reoperation, in the absence of other suitable conduits, RGEA is now used as secondary, tertiary, or quaternary arterial conduit to provide all-arterial revascularization. The biological

http://dx.doi.org/10.5772/54085

characteristics of RGEA are similar to IMA, but unclear benefits for third or fourth arterial grafts, the increment of surgery time, and the involvement of an additional body cavity are the main drawbacks limiting the widespread use of this conduit. Occasionally, the RGEA is used to supply the inferior cardiac wall and is anastomosed as an in situ graft to the posterior descending artery (PDA). In these cases, the mobilized artery is seen coursing anterior to the liver and through the diaphragm to reach the site of anastomosis. Small clips can be identified at the original site of the RGEA, near the small curvature of stomach. These instances require that the surgical history be conveyed to the radiologist so the CTA protocol can be modified to include the upper abdomen, because the gastroepiploic artery is freed to course anteriorly to the liver and through the diaphragm to reach the target vessel. The inferior epigastric artery (IEA) is an arterial branch of the abdominal wall, arising from the external iliac artery and coursing inside the abdominal rectus muscle. Similar to the radial artery (RA), the IEA has a predominant muscular structure, while the limited length of the vessel with an adequate caliber is a constraint to using this vessel only as a lateral branch of a multiple arterial graft.

4.3. Complication

4.3.1. Graft failure

Bypass graft failures are classified either as early or late following CABG surgery. During the early phase, usually within 1 month after CABG surgery, the most common cause of graft failure is thrombosis from platelet dysfunction at the site of focal endothelial damage during surgical harvesting and anastomosis. Graft closure from thrombosis at 1 month is a recognized complication in 10-15% of cases (Fitzgibbon et al., 1996). Perioperative venous graft failure after off-pump CABG procedures is chiefly determined by the two factors of graft endothelial damage and patient hypercoagulability. Early bypass graft failure can also be due to a malpositioned graft (Ricci et al., 2000). If the graft is too long, it may twist or kink. Technical factors associated with use of an aortic connector may predispose venous grafts to kinking (Traverse et al., 2003). Late-phase venous graft failure is due primarily to progressive changes related to systemic blood pressure exposure. One month after surgery, the venous graft starts to undergo neointimal hyperplasia. Although this process does not produce significant stenosis, it is the foundation for later development of graft atheroma. Beyond 1 year, atherosclerosis is the dominant process, resulting in graft stenosis and occlusion. On the other hand, arterial grafts, specifically IMA graft, are resistant to atheroma development. Late IMA graft failure is more commonly due to progression of atherosclerotic disease in the native coronary artery distal to the graft anastomosis. CTA can delineate multiple findings associated with graft stenosis and occlusion. Calcifiedand noncalcified atherosclerotic plaque is readily identified, and the calculation of the extent of graft narrowing is straightforward. Occlusion can be determined by non-visualization of a vessel which is known to have been used for surgical grafting. In many instances, the most proximal part of an occluded aortocoronary graft fills with contrast, creating a small out-pouching from the ascending aorta, allowing a diagnosis. Acute or chronic graft occlusion can

sometimes be differentiated by the diameter of the bypass graft. In chronic occlusion, the diameter is usually reduced from scarring, as compared with acute occlusion in which the diameter is usually enlarged.

4.3.2. Graft vasospasm

Radial artery (RA) grafts are susceptible to vasospasm because the RA is a muscular artery with elevated vasoreactivity. The appearance is similar to fixed graft stenosis, although the luminal narrowing is more extensive in length. Nevertheless, the administration of intraoperative alpha-adrenergic antagonist solution or posteroperative calcium channel blockers can overcome many cases of graft vasospasm postoperatively (Locker et al., 2002; Myers & Fremes, 2003).

4.3.3. Graft aneurysm

There are 2 types of bypass graft aneurysms: true aneurysms and pseudoaneurysms (Dubois & Vandervoort, 2001; Mohara et al., 1998). True aneuryms are usually found 5 to 7 years after CABG surgery and are related to atherosclerotic disease. On the other hand, pseudoaneuryms more commonly occur within 6 months after surgery, although they may also arise several years later. Pseudoaneurysms arise at either proximal or distal anastomotic sites. Pseudoaneurysm cases that are found earlier may be related to infection or tension at the anastomotic site, resulting in suture rupture. In late-onset pseudoaneurysms, similar to true aneurysms, atherosclerotic changes likely played a role. Currently, there is no clear guideline for surgery. Nevertheless, size >2 cm has been a cause for concern (Memon et al., 2003). Graft aneurysms may lead to various complications, including compression and mass effect on adjacent structures, thrombosis and embolization of the bypass graft leading to an acute coronary event, formation of fistula to the right atrium and ventricle, sudden rupture leading to hemothorax, hemopericardium, or death.

4.3.4. Pericardialand pleuraleffusions

Approximately 22%-85% of patients have postoperative pericardial effusions after CABG surgery (Meurin et al., 2004; Pepi et al., 1994). Although pericardial effusions are common, only 0.8%-6% of patients progress to cardiac temponade (Katara et al., 2003). Risk factors include postoperative coagulation abnormality or use of anticoagulation agents that are often related to the use of cardiopulmonary bypass. Nearly all significant pericardial effusions are diagnosed within 5 days postoperatively, peak in 10 days, and resolve within a month (Kuvin et al., 2002). Postoperative pleural effusions are even more numerous after surgery, a prevalence of 89% within 7 days after surgery (Hurlbut et al., 1990; Vargas et al., 1994). These pleural effusions are usually unilateral, small, left-sided, and without clinical significance. Only 1%-4% of CABG surgery patients proceed to develop clinically significant effusions that require thoracentesis (Peng et al., 1992).

http://dx.doi.org/10.5772/54085

4.3.5. Sternal infection

The sternal infection is an important complication of the CABG surgery, with a prevalence of 1% to 20% (Roy, 1998). Three different compartments may be affected: the presternal (cellulitis, sinus tracts, and abscess), sternal (osteomyelitis, and dehiscence), or retrosternal (mediastinitis, hematoma, and abscess) compartments (Li & Fishman, 2003). Risk factors include diabetes mellitus, obesity, current cigarette smoking, and steroid therapy. Surgical risk factors include complexity of surgery, type of bone saw used, type of sternal closure, length of surgical time, blood transfusions, and early reexploration to control hemorrhage. The CTA is important in revealing the extent and depth of infection, which, in turn, will help guide treatment planning. Usually, the preservation of mediastinalfat planes in CTA excludes surgical intervention. On the other hand, obliteration of mediastinalfat planes and diffuse soft tissue infiltration without or with gas collection, or low-density fluid collections within the mediastinum, are concerning for sternal infection. Recently published studies reported a 1-year mortality rate of approximately 22% (Loop et al., 1986; Sarr et al., 1984).

4.3.6. Pulmonary embolism

Clinical diagnosis of deep vein thrombosis and pulmonary embolism may be especially challenging because postoperative atelectasis, pleural effusion, or fluid overload may all contribute to the development of chest pain and dyspnea after CABG surgery. A recent report regarding pulmonary embolism in the post-CABG surgery population showed an overall prevalence of 23% for deep vein thrombosis by 1 week after surgery, with less than 2% of these cases identified clinically (Shammas, 2000).

4.3.7. Incidental findings

Although the intent of CTA after CABG surgery is to assess bypass graft patency and surgical complications, incidental findings are also frequently detected. In a recent study, 13.1% of patients in the immediate postoperative period had unsuspected noncardiac findings, including pulmonary embolism, pulmonary nodules, pneumonia, mucous plugging, and pneumothorax. (Mueller et al., 2007) Therefore, radiologists need to be aware of clinically significant findings with possible life-threatening consequences. 5. Conclusions

Despite image-degrading effects caused by the metallic scaffold of the stent, recent experience with the current generation of 64-section scanners suggests improved assessability of the in-stent lumen with the capability to appreciate more subtle degrees of in-stent neointimal hyperplasia. Knowledge of the different types of artifacts and how they can be compensated for with dedicated postprocessing and appropriate image views and window settings is a prerequisite for reliable depiction of the in-stent lumen and leads to a more robust application of CT findings. In future, the development of biodegradable stents may create optimal conditions for noninvasive post-implantation follow-up with MDCT. In recent years, MDCT with retrospective ECG gating has gained rapid acceptance as a diagnostic cardiac imaging modality, allowing assessment of coronary bypass graft patency with high spatial resolution. This tool could play an important role in patients with recurrence of chest pain

or with unclear stress test results after myocardial revascularization surgery. Therefore, it is crucial that cardiologists and radiologists understand CABG anatomy with knowledge of the type and number of bypass grafts used during myocardial revascularization surgery.

Author details

Bong Gun Song

Cardiovascular Imaging Center, Cardiac and Vascular Center, Konkuk University Medical Center, Republic of Korea

References

[1] Achenbach, S.; Moshage, W.; Ropers, D.; Nossen, J. & Bachmann, K. (1997). Noninvasive, three-dimensional visualization of coronary artery bypass grafts by electron beam tomography. *American Journal of Cardiology*, Vol.79, No.7, (Apr 1 1997), pp. 856-861, ISSN 0002-9149

[2] Alexopoulos D.; Xanthopoulou I. (2011). Coronary stent fracture: how frequent it is? Does it matter? *Hellenic J Cardiol*, Vol.52, No.1, pp. 1-5, ISSN 1109-9666

[3] Anders, K.; Baum, U.; Schmid, M.; Ropers, D.; Schmid, A.; Pohle, K.; Daniel, W. G.; Bautz, W. & Achenbach, S. (2006). Coronary artery bypass graft (CABG) patency: assessment with high-resolution submillimeter 16-slice multidetector-row computed tomography (MDCT) versus coronary angiography. *European Journal of Radiology*, Vol.57, No.3, (Mar 2006), pp. 336-344, ISSN 0720-048X

[4] Bourassa, M. G.; Fisher, L. D.; Campeau, L.; Gillespie, M. J.; McConney, M. & Lesperance, J. (1985). Long-term fate of bypass grafts: the Coronary Artery Surgery Study (CASS) and Montreal Heart Institute experiences. *Circulation*, Vol.72, No.6 Pt 2, (Dec 1985), pp. V71-78, ISSN 0009-7322

[5] Buche, M.; Schoevaerdts, J. C.; Louagie, Y.; Schroeder, E.; Marchandise, B.; Chenu, P.; Dion, R.; Verhelst, R.; Deloos, M.; Gonzales, E. & et al. (1992). Use of the inferior epigastric artery for coronary bypass. *Journal of Thoracic and Cardiovascular Surgery*, Vol. 103, No.4, (Apr 1992), pp. 665-670, ISSN 0022-5223

[6] Campeau, L.; Enjalbert, M.; Lesperance, J.; Vaislic, C.; Grondin, C. M. & Bourassa, M. G. (1983). Atherosclerosis and late closure of aortocoronary saphenous vein grafts: sequential angiographic studies at 2 weeks, 1 year, 5 to 7 years, and 10 to 12 years after surgery. *Circulation,* Vol.68, No.3 Pt 2, (Sep 1983), pp. II1-7, ISSN 0009-7322

[7] Carpentier, A.; Guermonprez, J. L.; Deloche, A.; Frechette, C. & DuBost, C. (1973). The aorta-to-coronary radial artery bypass graft. A technique avoiding pathological

changes in grafts. *Annals of Thoracic Surgery*, Vol.16, No.2, (Aug 1973), pp. 111-121, ISSN 0003-4975

[8] Carrel, T. P.; Eckstein, F. S.; Englberger, L.; Windecker, S. & Meier, B. (2003). Pitfalls and key lessons with the symmetry proximal anastomotic device in coronary artery bypass surgery. *Annals of Thoracic Surgery*, Vol.75, No.5, (May 2003), pp. 1434-1436, ISSN 0003-4975

[9] Chiurlia E.; Menozzi M.; Ratti C.; Romagnoli R.; Modena MG. (2005). Follow-up of coronary artery bypass graft patency by multislice computed tomography. *Am J Cardiol*, Vol.95, No.9, pp 1094-1097, ISSN 0002-9149

[10] Dikkers, R.; Willems, T. P.; Tio, R. A.; Anthonio, R. L.; Zijlstra, F. & Oudkerk, M. (2007). The benefit of 64-MDCT prior to invasive coronary angiography in symptomatic post-CABG patients. *International Journal of Cardiovascular Imaging,* Vol.23, No. 3, (Jun 2007), pp. 369-377, ISSN 1569-5794

[11] Dubois, C. L. & Vandervoort, P. M. (2001). Aneurysms and pseudoaneurysms of coronary arteries and saphenous vein coronary artery bypass grafts: a case report and literature review. Acta Cardiologica, Vol.56, No.4, (Aug 2001), pp. 263-267, ISSN 0001-5385

[12] Engelmann, M. G.; von Smekal, A.; Knez, A.; Kurzinger, E.; Huehns, T. Y.; Hofling, B. & Reiser, M. (1997). Accuracy of spiral computed tomography for identifying arterial and venous coronary graft patency. *American Journal of Cardiology,* Vol.80, No.5, (Sep 1 1997), pp. 569-574, ISSN 0002-9149

[13] Fitzgibbon, G. M.; Kafka, H. P.; Leach, A. J.; Keon, W. J.; Hooper, G. D. & Burton, J. R. (1996). Coronary bypass graft fate and patient outcome: angiographic follow-up of 5,065 grafts related to survival and reoperation in 1,388 patients during 25 years. *Journal of the American College of Cardiology*, Vol.28, No.3, (Sep 1996), pp. 616-626, ISSN 0735-1097

[14] Frazier, A. A.; Qureshi, F.; Read, K. M.; Gilkeson, R. C.; Poston, R. S. & White, C. S. (2005). Coronary artery bypass grafts: assessment with multidetector CT in the early and late postoperative settings. *Radiographics*, Vol.25, No.4, (Jul-Aug 2005), pp. 881-896, ISSN 1527-1323

[15] Fullerton, D. A.; St Cyr, J. A.; Fall, S. M. & Whitman, G. J. (1994). Protection of the patent internal mammary artery by-pass graft from subsequent sternotomy. *Journal of Cardiovascular Surgery*, Vol.35, No.6, (Dec), pp. 499-501, ISSN 0021-9509

[16] Gilkeson, R. C.; Markowitz, A. H. & Ciancibello, L. (2003). Multisection CT evaluation of the reoperative cardiac surgery patient. *Radiographics*, Vol.23 Spec No, (Oct 2003), pp. S3-17, ISSN 1527-1323

[17] Gillinov, A. M.; Casselman, F. P.; Lytle, B. W.; Blackstone, E. H.; Parsons, E. M.; Loop, F. D. & Cosgrove, D. M., 3rd (1999). Injury to a patent left internal thoracic artery

graft at coronary reoperation. *Annals of Thoracic Surgery*, Vol.67, No.2, (Feb 1999), pp. 382-386, ISSN 0003-4975

[18] Gilard M, Cornily JC, Pennec PY, Le Gal G, Nonent M, Mansourati J, Blanc JJ, Boschat J. (2006). Assessment of coronary artery stents by 16 slice computed tomography. *Heart*, Vol.92, No.1, (Jan 2006), pp.58-61, ISSN 1468-201X

[19] Hecht, H. S. & Roubin, G. (2007). Usefulness of computed tomographic angiography guided percutaneous coronary intervention. *American Journal of Cardiology*, Vol.99, No.6, (Mar 15 2007), pp. 871-875, ISSN 0002-9149

[20] Hurlbut, D.; Myers, M. L.; Lefcoe, M. & Goldbach, M. (1990). Pleuropulmonary morbidity: internal thoracic artery versus saphenous vein graft. *Annals of Thoracic Surgery*, Vol.50, No.6, (Dec 1990), pp. 959-964, ISSN 0003-4975

[21] Katara, A. N.; Samra, S. S. & Bhandarkar, D. S. (2003). Thoracoscopic window for a post-coronary artery bypass grafting pericardial effusion. *Indian Heart Journal*, Vol.55, No.2, (Mar-Apr 2003), pp. 180-181, ISSN 0019-4832

[22] Kitagawa T.; Fujii T.; Tomohiro Y.; Maeda K.; Kobayashi M.; Kunita E.; Sekiguchi Y. (2006). Noninvasive assessment of coronary stents in patients by 16-slice computed tomography. *Int J Cardiol*, Vol.109, No.2, (Jul 2005), pp. 188-194, ISSN 0167-5273

[23] Kuvin, J. T.; Harati, N. A.; Pandian, N. G.; Bojar, R. M. & Khabbaz, K. R. (2002). Postoperative cardiac tamponade in the modern surgical era. *Annals of Thoracic Surgery*, Vol.74, No.4, (Oct 2002), pp. 1148-1153, ISSN 0003-4975

[24] Lee, R.; Lim, J.; Kaw, G.; Wan, G.; Ng, K. & Ho, K. T. (2010). Comprehensive noninvasive evaluation of bypass grafts and native coronary arteries in patients after coronary bypass surgery: accuracy of 64-slice multidetector computed tomography compared to invasive coronary angiography. *Journal of Cardiovascular Medicine (Hagerstown),* Vol.11, No.2, (Feb 2010), pp. 81-90, ISSN 1558-2035

[25] Leipsic J.; Labounty TM.; Heilbron B.; Min JK.; Mancini GB.; Lin FY.; Taylor C.; Dunning A.; Earls JP. (2010). Adaptive statistical iterative reconstruction: assessment of image noise and image quality in coronary CT angiography. *AJR Am J Roentgenol*, Vol.195, No.3, pp. 649-54, ISSN 1546-3141

[26] Li, A. E. & Fishman, E. K. (2003). Evaluation of complications after sternotomy using single- and multidetector CT with three-dimensional volume rendering. *AJR. American Journal of Roentgenology*, Vol.181, No.4, (Oct 2003), pp. 1065-1070, ISSN 0361-803X

[27] Lim HB.; Hur G.; Kim SY.; Kim YH.; Kwon SU.; Lee WR.; Cha SJ. (2008). Coronary stent fracture: detection with 64-section multidetector CT angiography in patients and in vitro. Radiology, Vol.249, No.3, pp. 810-819, ISSN 1527-1323

[28] Locker, C.; Mohr, R.; Paz, Y.; Lev-Ran, O.; Herz, I.; Uretzky, G. & Shapira, I. (2002). Pretreatment with alpha-adrenergic blockers for prevention of radial artery spasm. *Annals of Thoracic Surgery*, Vol.74, No.4, (Oct 2002), pp. S1368-1370, ISSN 0003-4975

[29] Loop, F. D.; Lytle, B. W.; Cosgrove, D. M.; Stewart, R. W.; Goormastic, M.; Williams, G. W.; Golding, L. A.; Gill, C. C.; Taylor, P. C.; Sheldon, W. C. & et al. (1986). Influence of the internal-mammary-artery graft on 10-year survival and other cardiac events. *New England Journal of Medicine*, Vol.314, No.1, (Jan 1986), pp. 1-6, ISSN 0028-4793

[30] Mack, M. J.; Emery, R. W.; Ley, L. R.; Cole, P. A.; Leonard, A.; Edgerton, J. R.; Dewey, T. M.; Magee, M. J. & Flavin, T. S. (2003). Initial experience with proximal anastomoses performed with a mechanical connector. *Annals of Thoracic Surgery*, Vol.75, No.6, (Jun 2003), pp. 1866-1870; discussion 1870-1871, ISSN 0003-4975

[31] Mahnken AH.; Mühlenbruch G.; Seyfarth T.; Flohr T.; Stanzel S.; Wildberger JE.; Günther RW.; Kuettner A. (2006). 64-slice computed tomography assessment of coronary artery stents: a phantom study. *Acta Radiol*, Vol. 47, No.1, pp. 36-42, ISSN 0284-1851

[32] Maintz D.; Burg MC.; Seifarth H.; Bunck AC.; Ozgün M.; Fischbach R.; Jürgens KU.; Heindel W. (2009). Update on multidetector coronary CT angiography of coronary stents: in vitro evaluation of 29 different stent types with dual-source CT. *Eur Radiol*, Vol.19, No.1, pp. 42-49, ISSN 1432-1084

[33] Maintz D.; Seifarth H.; Flohr T.; Krämer S.; Wichter T.; Heindel W.; Fischbach R. (2003). Improved coronary artery stent visualization and in-stent stenosis detection using 16-slice computed-tomography and dedicated image reconstruction technique. *Invest Radiol*, Vol.38, No.12, pp.790-795, ISSN 0020-9996

[34] Manapat, A. E.; McCarthy, P. M.; Lytle, B. W.; Taylor, P. C.; Loop, F. D.; Stewart, R. W.; Rosenkranz, E. R.; Sapp, S. K.; Miller, D. & Cosgrove, D. M. (1994). Gastroepiploic and inferior epigastric arteries for coronary artery bypass. Early results and evolving applications. *Circulation*, Vol.90, No.5 Pt 2, (Nov 1994), pp. II144-147, ISSN 0009-7322

[35] Marano, R.; Storto, M. L.; Maddestra, N. & Bonomo, L. (2004). Non-invasive assessment of coronary artery bypass graft with retrospectively ECG-gated four-row multidetector spiral computed tomography. *European Radiology*, Vol.14, No.8, (Aug 2004), pp. 1353-1362, ISSN 0938-7994

[36] Marano, R.; Storto, M. L.; Merlino, B.; Maddestra, N.; Di Giammarco, G. & Bonomo, L. (2005). A pictorial review of coronary artery bypass grafts at multidetector row CT. *Chest*, Vol.127, No.4, (Apr 2005), pp. 1371-1377, ISSN 0012-3692

[37] Memon, A. Q.; Huang, R. I.; Marcus, F.; Xavier, L. & Alpert, J. (2003). Saphenous vein graft aneurysm: case report and review. *Cardiology in Review*, Vol.11, No.1, (Jan-Feb 2003), pp. 26-34, ISSN 1061-5377

[38] Meurin, P.; Weber, H.; Renaud, N.; Larrazet, F.; Tabet, J. Y.; Demolis, P. & Ben Driss, A. (2004). Evolution of the postoperative pericardial effusion after day 15: the problem of the late tamponade. *Chest*, Vol.125, No.6, (Jun 2004), pp. 2182-2187, ISSN 0012-3692

[39] Min JK.; Swaminathan RV.; Vass M.; Gallagher S.; Weinsaft JW. (2009). High-definition multidetector computed tomography for evaluation of coronary artery stents: comparison to standard-definition 64-detector row computed tomography. *J Cardiovasc Comput Tomogr*, Vol.3, No.4, (Jul-Aug 2009), pp. 246-251, ISSN 1876-861X

[40] Mohara, J.; Konishi, H.; Kato, M.; Misawa, Y.; Kamisawa, O. & Fuse, K. (1998). Saphenous vein graft pseudoaneurysm rupture after coronary artery bypass grafting. *Annals of Thoracic Surgery*, Vol.65, No.3, (Mar 1998), pp. 831-832, ISSN 0003-4975

[41] Motwani, J. G. & Topol, E. J. (1998). Aortocoronary saphenous vein graft disease: pathogenesis, predisposition, and prevention. *Circulation*, Vol.97, No.9, (Mar 10 1998), pp. 916-931, ISSN 0009-7322

[42] Mueller, J.; Jeudy, J.; Poston, R. & White, C. S. (2007). Cardiac CT angiography after coronary bypass surgery: prevalence of incidental findings. *AJR. American Journal of Roentgenology*, Vol.189, No.2, (Aug 2007), pp. 414-419, ISSN 1546-3141

[43] Muneretto, C.; Bisleri, G.; Negri, A.; Manfredi, J.; Metra, M.; Nodari, S.; Culot, L. & Dei Cas, L. (2003). Total arterial myocardial revascularization with composite grafts improves results of coronary surgery in elderly: a prospective randomized comparison with conventional coronary artery bypass surgery. *Circulation*, Vol.108 Suppl 1, (Sep 2003), pp. II29-33, ISSN 1524-4539

[44] Myers, M. G. & Fremes, S. E. (2003). Prevention of radial artery graft spasm: a survey of Canadian surgical centres. *Canadian Journal of Cardiology*, Vol.19, No.6, (May 2003), pp. 677-681, ISSN 0828-282X

[45] Nakazawa G.; Finn AV.; Vorpahl M.; Ladich E.; Kutys R.; Balazs I.; Kolodgie FD.; Virmani R. (2009). Incidence and predictors of drug-eluting stent fracture in human coronary artery a pathologic analysis. *J Am Coll Cardiol*, Vol.54, No.21, (Nov 2009), pp.1924-1931, ISSN 1558-3597

[46] Nieman K.; Pattynama PM.; Rensing BJ.; Van Geuns RJ.; De Feyter PJ. (2003). Evaluation of patients after coronary artery bypass surgery: CT angiographic assessment of grafts and coronary arteries. *Radiology*, Vol.229, No.3, (Dec 2003), pp.749-756, ISSN 0033-8419

[47] Ohtsuka, T.; Akahane, M.; Ohtomo, K.; Kotsuka, Y. & Takamoto, S. (2000). Three-dimensional computed tomography for reoperative minimally invasive coronary artery bypass. *Annals of Thoracic Surgery*, Vol.70, No.5, (Nov 2000), pp. 1734-1735, ISSN 0003-4975

[48] Pang JH.; Kim D.; Beohar N.; Meyers SN.; Lloyd-Jones D.; Yaghmai V. (2009). Detection of stent fractures: a comparison of 64-slice CT, conventional cine-angiography, and intravascular ultrasonography. *Acad Radiol*, Vol.16, No.4, (Apr 2009), pp.412-417, ISSN 1878-4046

[49] Peng, M. J.; Vargas, F. S.; Cukier, A.; Terra-Filho, M.; Teixeira, L. R. & Light, R. W. (1992). Postoperative pleural changes after coronary revascularization. Comparison

between saphenous vein and internal mammary artery grafting. *Chest,* Vol.101, No.2, (Feb 1992), pp. 327-330, ISSN 0012-3692

[50] Pepi, M.; Muratori, M.; Barbier, P.; Doria, E.; Arena, V.; Berti, M.; Celeste, F.; Guazzi, M. & Tamborini, G. (1994). Pericardial effusion after cardiac surgery: incidence, site, size, and haemodynamic consequences. *British Heart Journal,* Vol.72, No.4, (Oct 1994), pp. 327-331, ISSN 0007-0769

[51] Possati, G.; Gaudino, M.; Prati, F.; Alessandrini, F.; Trani, C.; Glieca, F.; Mazzari, M. A.; Luciani, N. & Schiavoni, G. (2003). Long-term results of the radial artery used for myocardial revascularization. *Circulation*, Vol.108, No.11, (Sep 2003), pp. 1350-1354, ISSN 1524-4539

[52] Poston, R.; White, C.; Read, K.; Gu, J.; Lee, A.; Avari, T. & Griffith, B. (2004). Virchow triad, but not use of an aortic connector device, predicts early graft failure after off-pump coronary bypass. *Heart Surg Forum*, Vol.7, No.5, pp. E428-433, ISSN 1522-6662

[53] Pugliese F.; Cademartiri F.; van Mieghem C.; Meijboom WB.; Malagutti P.; Mollet NR.; Martinoli C.; de Feyter PJ.; Krestin GP. (2006). Multidetector CT for visualization of coronary stents. *Radiographics*, Vol.26, No.3, (May-Jun 2006), pp.887-904,

[54] Pym, J.; Brown, P. M.; Charrette, E. J.; Parker, J. O. & West, R. O. (1987). Gastroepiploic-coronary anastomosis. A viable alternative bypass graft. *Journal of Thoracic and Cardiovascular Surgery*, Vol.94, No.2, (Aug 1987), pp. 256-259, ISSN 0022-5223

[55] Rajiah P.; Schoenhagen P.; Mehta D.; Ivanc T.; Lieber M.; Soufan K.; Desai M.; Flamm SD.; Halliburton S. (2012). Low-dose, wide-detector array thoracic aortic CT angiography using an iterative reconstruction technique results in improved image quality with lower noise and fewer artifacts. *J Cardiovasc Comput Tomogr*, Vol.6, No.3, (May 2012), pp.205-213, ISSN 1876-861X

[56] Ricci, M.; Karamanoukian, H. L.; D'Ancona, G.; Salerno, T. A. & Bergsland, J. (2000). Reoperative "off-pump" circumflex revascularization via left thoracotomy: how to prevent graft kinking. *Annals of Thoracic Surgery*, Vol.70, No.1, (Jul 2000), pp. 309-310, ISSN 0003-4975

[57] Ropers, D.; Pohle, F. K.; Kuettner, A.; Pflederer, T.; Anders, K.; Daniel, W. G.; Bautz, W.; Baum, U. & Achenbach, S. (2006). Diagnostic accuracy of noninvasive coronary angiography in patients after bypass surgery using 64-slice spiral computed tomography with 330-ms gantry rotation. *Circulation*, Vol.114, No.22, (Nov 2006), pp. 2334-2341; quiz 2334, ISSN 1524-4539

[58] Ropers, D.; Ulzheimer, S.; Wenkel, E.; Baum, U.; Giesler, T.; Derlien, H.; Moshage, W.; Bautz, W. A.; Daniel, W. G.; Kalender, W. A. & Achenbach, S. (2001). Investigation of aortocoronary artery bypass grafts by multislice spiral computed tomography with electrocardiographic-gated image reconstruction. *American Journal of Cardiology*, Vol.88, No.7, (Oct 2001), pp. 792-795, ISSN 0002-9149

[59] Roy, M. C. (1998). Surgical-site infections after coronary artery bypass graft surgery: discriminating site-specific risk factors to improve prevention efforts. *Infection Control and Hospital Epidemiology*, Vol.19, No.4, (Apr 1998), pp. 229-233, ISSN 0899-823X

[60] Sarr, M. G.; Gott, V. L. & Townsend, T. R. (1984). Mediastinal infection after cardiac surgery. *Annals of Thoracic Surgery*, Vol.38, No.4, (Oct 1984), pp. 415-423, ISSN 0003-4975

[61] Schlosser, T.; Konorza, T.; Hunold, P.; Kuhl, H.; Schmermund, A. & Barkhausen, J. (2004). Noninvasive visualization of coronary artery bypass grafts using 16-detector row computed tomography. *Journal of the American College of Cardiology*, Vol.44, No.6, (Sep 2004), pp. 1224-1229, ISSN 0735-1097

[62] Seifarth, H.; Raupach, R.; Schaller, S.; Fallenberg, E. M.; Flohr, T.; Heindel, W.; Fischbach, R. & Maintz, D. (2005). Assessment of coronary artery stents using 16-slice MDCT angiography: evaluation of a dedicated reconstruction kernel and a noise reduction filter. *European Radiology*, Vol.15, No.4, (Apr 2005), pp. 721-726, ISSN 0938-7994

[63] Seifarth H.; Ozgün M.; Raupach R.; Flohr T.; Heindel W.; Fischbach R.; Maintz D. (2006). 64- Versus 16-slice CT angiography for coronary artery stent assessment: in vitro experience. *Invest Radiol*, Vol.41, No.1, (Jan 2006), pp.22-27, ISSN 0020-9996

[64] Shammas, N. W. (2000). Pulmonary embolus after coronary artery bypass surgery: a review of the literature. *Clinical Cardiology*, Vol.23, No.9, (Sep 2000), pp. 637-644, ISSN 0160-9289

[65] Song, B. G.; Choi, J. H.; Choi, S. M.; Park, J. H.; Park, Y. H. & Choe, Y. H. (2010). Coronary artery graft dilatation aided by multidetector computed tomography. *Asian Cardiovascular and Thoracic Annals*, Vol.18, No.2, (Feb 2010), pp. 177-179, ISSN 1816-5370

[66] Tochii, M.; Takagi, Y.; Anno, H.; Hoshino, R.; Akita, K.; Kondo, H. & Ando, M. (2010). Accuracy of 64-slice multidetector computed tomography for diseased coronary artery graft detection. *Annals of Thoracic Surgery*, Vol.89, No.6, (Jun 2010), pp. 1906-1911, ISSN 1552-6259

[67] Traverse, J. H.; Mooney, M. R.; Pedersen, W. R.; Madison, J. D.; Flavin, T. F.; Kshettry, V. R.; Henry, T. D.; Eales, F.; Joyce, L. D. & Emery, R. W. (2003). Clinical, angiographic, and interventional follow-up of patients with aortic-saphenous vein graft connectors. *Circulation*, Vol.108, No.4, (Jul 2003), pp. 452-456, ISSN 1524-4539

[68] Ueyama, K.; Ohashi, H.; Tsutsumi, Y.; Kawai, T.; Ueda, T. & Ohnaka, M. (1999). Evaluation of coronary artery bypass grafts using helical scan computed tomography. *Catheterization and Cardiovascular Interventions*, Vol.46, No.3, (Mar 1999), pp. 322-326, ISSN 1522-1946

[69] Vargas, F. S.; Cukier, A.; Hueb, W.; Teixeira, L. R. & Light, R. W. (1994). Relationship between pleural effusion and pericardial involvement after myocardial revascularization. *Chest*, Vol.105, No.6, (Jun 1994), pp. 1748-1752, ISSN 0012-3692

[70] Vembar, M.; Garcia, M. J.; Heuscher, D. J.; Haberl, R.; Matthews, D.; Bohme, G. E. & Greenberg, N. L. (2003). A dynamic approach to identifying desired physiological phases for cardiac imaging using multislice spiral CT. *Medical Physics*, Vol.30, No.7, (Jul 2003), pp. 1683-1693, ISSN 0094-2405

[71] Wiklund, L.; Bugge, M. & Berglin, E. (2002). Angiographic results after the use of a sutureless aortic connector for proximal vein graft anastomoses. *Annals of Thoracic Surgery*, Vol.73, No.6, (Jun 2002), pp. 1993-1994, ISSN 0003-4975

IntechOpen